WIRELESS POWERED FLEXIBLE GASTROSTIMULATOR

A Dissertation

Submitted to the Faculty

of

University of Texas at Arlington

by

Souvik Dubey

In Partial Fulfillment of the

Requirements for the Degree

of

Doctor of Philosophy

May 2018

University of Texas at Arlington

Arlington, Texas

THE UNIVERSITY OF TEXAS AT ARLINGTON
GRADUATE SCHOOL
STATEMENT OF DISSERTATION APPROVAL

Dr. Jonathan Bredow, Chair

Department of Electrical Engineering

Dr. Wei-Jen Lee, Professor

Department of Electrical Engineering

Dr. Yuze Sun, Assistant Professor

Department of Electrical Engineering

Dr. Yuan B Peng, Professor

Department of Psychology

Approved by:

Dr. J.-C. Chiao, Supervising Professor

Department of Electrical Engineering

ACKNOWLEDGMENTS

I would like to express my appreciation and gratefulness to my supervising professor and mentor Dr. Jung-Chih Chiao. This thesis could not have written without his guidance, counseling, and sustenance. His buttress and encouragement thought out the period helped me to achieve the destination. I am thankful to Dr. Yuan B Peng and Dr. Gregory O'Grady for helping with the animal experiments. I also like to thank Dr. Bredow, Dr. Lee and Dr. Sun for being on my thesis committee.

A special thanks to all my friends in UTA and to all my colleagues of the iMEMS group, for being there by my side. Apart from learning technical knowledge, I have gained a lot of life experiences during my Ph.D. at UTA.

Finally, I would say my journey to this point would have been impossible without the blessing from my parents Mr. Sanjiban Kumar Dubey and Mrs. Nupur Dubey and my uncle Mr. Debashis Dubey. They believed in me and my abilities and encouraged me at every step to pursue my dreams.

TABLE OF CONTENTS

Page

LIST OF TABLES

LIST OF FIGURES

Figure Page

Figure Page

Figure Page

ABSTRACT

Dubey, Souvik Ph.D., University of Texas at Arlington, May 2018. Wireless Powered Flexible Gastrostimulator. Major Professor: J.-C. Chiao.

Gastric electrical stimulation (GES) is an effective alternative to long-term dietary and medicinal treatment for gastroparesis. This work presents the design and development of two miniature implantable battery-less gastrostimulators, operated by wireless radio-frequency power. The devices deliver controlled electrical pulses to the stomach tissues to help regain normal motility.

The first prototype was designed with the goal to optimize the wireless power transfer efficiency, various antenna configurations were investigated. The attenuation due to human tissue barrier was examined with an equivalent model. To enable reconfiguring the device to meet the patients' needs after implantation, a novel method of changing the settings without an additionally dedicated wireless communication channel has been proposed and demonstrated in this work.

The second prototype was a flexible gastrostimulator. The device was designed with energy harvesting antenna on one side and stimulation electrodes with the circuit on the other side. The wireless power transfer performances through air and animal tissues were investigated. The effect of antenna misalignment and bending were considered and validated for reliable wireless energy harvesting. The safety of wireless power transfer was shown with a long exposure temperature study. Finally, world's first flexible gastrostimulator was demonstrated with animal studies in rat and porcine model.

1. INTRODUCTION

1.1 Motivation

With a rapid increase in the number of patients diagnosed with gastric motility disorder in last few years, gastroparesis(GP) has become a global issue. Food is an integral part of the society and patients diagnosed with GP leads to very painful life since, consumption of solid food causes abdominal bloating, pain, nausea. GP patients, typically survive with liquid diet and for severe cases requires tube feeding and hospitalization. In spite of recent advances in medical treatments, use of gastric electrical stimulation (GES) was not successful to eradicate this endemic. A battery operated gastric electrical stimulator, Enterra Therapy (Medtronic Inc, MS) has found to be promising for alleviating the GP symptoms. However, large medical bills, prolonged and repeated hospitalizations were major contributing factors, adding the limitation to the GES treatment.

Due to recent advances in wireless technology, wireless power has gained a lot of attention from various fields. We have already seen wireless charger making into the market for household applications and electronic vehicles. Wireless power for medical implants shows tremendous potential due to the form factor reduction by removing the battery. Additionally, multiple battery replacement surgeries could be avoided with the wireless power approach. Reducing the size of the gastrostimulator could play a game-changing role in GES treatment since the stimulator could be implanted by minimally invasive surgery or endoscopic process. On the other side, the wireless power harvesting performance drops significantly with reduction of the implant antenna size. To solve this conundrum, the concept of the flexible gastric stimulator is introduced. The flexibility of the device provides an opportunity to roll the gastrostimulator into a smaller form factor so that, it could be delivered using

endoscopic process and once the device has been released from the endoscopic guide tube, it could come back to its relaxed state to efficiently harvest wireless energy with a larger cross-sectional area.

1.2 Objective

The objectives behind the design of flexible wirelessly powered miniature gastric stimulator were as follows:

- To design a miniature stimulation device to treat gastroparesis.
- To fabricate such a stimulation device which is flexible and can be rolled to change its form factor.
- To design a such a stimulation device which can operate without a battery using wireless power from outside body.
- To characterize the performance of the wireless power transfer system for various parameters like the effect of distance, misalignment and tissue attenuation.
- To investigate the safety of animal tissue during wireless power transfer for medical implants.
- To investigate the feasibility of flexible gastrostimulator placement in the sub-mucosal place of the stomach.
- To investigate the feasibility of implanting the flexible gastrostimulator using an endoscopic process.

1.3 Thesis Organization

The thesis is organized and divided into six chapters for better readability and understanding. The detailed information about the gastric electrical stimulation is given in Chapter 2. Its also describes what are the existing treatment methods of

gastroparesis and challenges associated with those approaches. It also introduces proposed flexible gastric stimulator and explains how it is better than existing system and also addresses the challenges as described in the previous section.

Chapter 3 elucidates the system design, the overall system design has 3 sections. In the first section, the concept of wireless power transfer(WPT) has been described for rigid gastrostimulator along with antenna design, WPT circuit design and characterization process of the WPT link. The communication protocol between the implant and the transmitter and the remote reconfiguration of the implant are also discussed in this section. The second section explains the concept, antenna design, circuit design and the fabrication process for flexible gastrostimulator. The required stimulation parameters for gastric electrical stimulation are discussed in the final section of this chapter.

The experimental results are given in chapter 4. The details for benchtop experimental setups are discussed in this chapter. Various characterization techniques are explained with experimental results. The effects of distance, antenna type, resonance frequency, misalignment on WPT link performances are presented in this section. Several investigation results are given to study the effect of dielectric layers in between transmitter and receiver antennas. Tissue safety experiments are also concluded for long duration WPT for medical devices. This section also includes results for stimulation pulses at various settings and remote re-configuration of the implant using communication algorithm as proposed chapter 3.

Chapter 5 presents the animal experiments results. Two different animal experiments results are presented in this section. Muscle stimulation is demonstrated in rat model using flexible gastric stimulator powered wirelessly. Stimulation readings were recorded. The viability of implanting flexible gastrostimulator in the submucosal space was investigated in a porcine model and discussed in this section.

Finally, chapter 6 summarizes the research results, draws the conclusion and provides insight on the future work. Additionally, stomach motility tracking feature

also included for future work which could be useful to find out the efficacy of the stimulation therapy in real time.

2. GASTROPARESIS AND GASTRIC ELECTRICAL STIMULATION

2.1 Background

The word gastroparesis is derived from the Greek words gastro and pa'resis which translates to paralysis of the stomach. As the name suggests the diagnosis of the gastroparesis is defined as the delayed gastric emptying of a solid meal in the absence of mechanical obstructions. Gastroparesis (GP) patients suffer from one or more following symptoms: postprandial fullness, early satiety, nausea, vomiting, abdominal bloating and pain. In addition, the societal impact of the GP is significant. These symptoms worsen with poor food intake and lead to weight loss, malnutrition, impaired function, and more emergency room visits. It is considered to be one of the major health problem affecting 10% to 15% of the population globally [1]. The number of gastroparesis cases in the USA alone has increased alarmingly since, it is caused due to diseases like cancer, diabetes and Parkinson's disease. At the year 2013 in the USA only, there were 16460 admissions with a principal discharge diagnosis of gastroparesis as compared to 3978 cases in 1997 [2]. The net spending on hospital bills due to gastroparesis increased exponentially by 1026% from \$50456642 $\pm$ 4662620 in 1997 to \$568417666 $\pm$ 22374060 in 2013 [2]. The data also suggest the number of hospital admission for GP in the USA now surpassed those for gastroesophageal reflux, gastritis, nausea and peptic ulcer disease [3].

2.2 Gastroparesis

Gastroparesis is characterized as one of the gastric dysrhythmia resulting delayed emptying of a solid meal. It is correlated with the abnormal gastric myoelectric

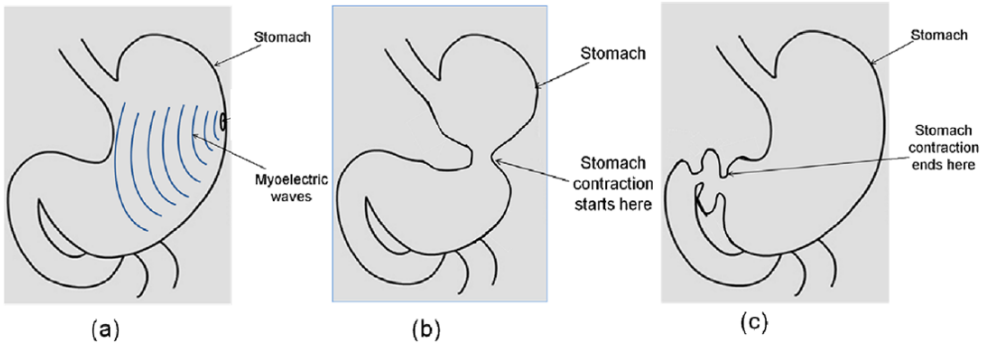

Fig. 2.1. Myoelectric activity of the stomach, (a) Slow waves are generated from the corpus within stomach, (b) Stomach contraction and the slow wave transmission, (c) End point of the stomach contraction [4].

activity which can be further explained as abnormal slow-wave frequency, low slow-wave amplitude, and slow-wave uncoupling. These conditions are also known as Bradygastrias or gastric hypo-motility and uncoordinated gastric contractions are called Tachygastrias [5].

The peristaltic contraction in the stomach is a major responsible factor for movement of the solid food within the stomach. The contraction originates from the corpus region which is the largest part of the stomach and propagates down to the pyloric region producing a push to propel the semi-digested food into the intestine through the pyloric canal. The peristaltic movements are resultant of the slow waves generated by a dense network of electrically coupled Interstitial Cells of Cajal (ICC) present in between circular and longitudinal smooth muscle cells of the stomach wall. There are primarily four layers in the stomach wall and these are starting from the innermost layer, named mucosa, sub-mucosa, muscularis externa and the serosa. The muscularis externa is made of an inner circular layer of smooth muscles and a less developed outer longitudinal layer whereas, serosa is formed with simple squamous epithelium. The inner layer of the stomach is known as mucosa which is composed of epithelium, lamina propria, and a muscularis mucosa. Like serosa, muscularis mucosa has smooth

muscle cells in the inner circular and outer longitudinal layers. The generation of slow wave is shown in Fig. 2.1(a) and subsequent propagation of stomach contractions and relaxations are shown in Fig. 2.1(b) and (c).

There are several factors which lead to GP, patients with diabetes mellitus, gastric surgery and cancer are the most vulnerable to get GP. In some cases, GP is also considered idiopathic, when exact factors that lead to GP cannot be identified. It has been found that for idiopathic GP cases, a large number of patients have had previous gastrointestinal tract viral infection [5].

2.3 Popular Treatments

Paucity of the currently available treatment options makes it more challenging to treat patients with GP. Medical management of GP is limited to prokinetic therapy combined with antiemetic agents, nutritional support (e.g., oral caloric supplementation, enteral tube feeding with a jejunostomy, or total parenteral nutrition) and pain management [5]. Prokinetic agents stimulate gastric motility and coordinate gastric-duodenal motor activities. Few prokinetic drugs are metoclopramide, erythromycin, cisapride and domperidone. However, in the USA metoclopramide and erythromycin are the only commercially available drugs for GP. These drugs have serious side effects which make them intolerable for 40% of the patients [6] and also found to be less effective for chronic GP patients. Partial or complete gastrectomy is regarded as the final option since it is associated with mortality and morbidity [7].

Gastric electrical stimulation (GES) holds the potential for treating not only gastroparesis but also eating disorders, such as morbid obesity. The electrical stimulation is applied to the smooth muscle cells of the serosa or the mucosa by an implantable device which works like a pacemaker for the stomach, like a heart pacemaker, it controls the motility of the stomach muscle by adjusting characteristics of the electrical stimulation pulses. Depending on the device settings, GES can enhance or inhibit stomach muscle contraction, and therefore be able to alter the emptying time of the

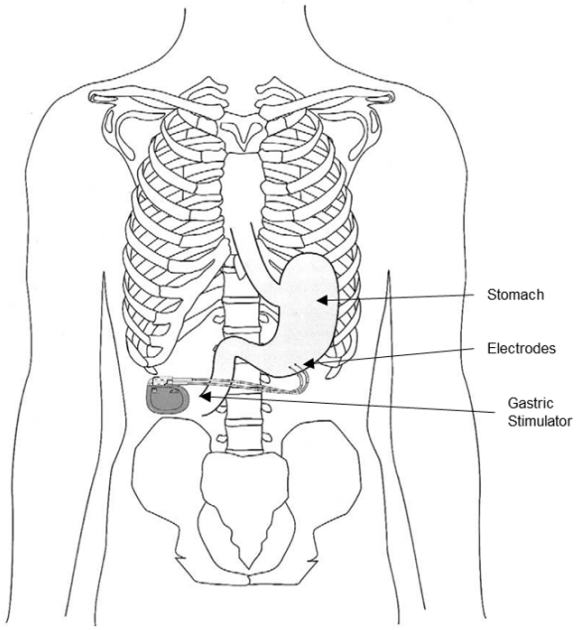

Fig. 2.2. Existing gastric electrical stimulation (GES) system and its location. The GES unit comprised a pair of leads secured in the muscularis propria along the greater curvature, 10 cm proximal to the pylorus, 1 cm apart, and connected to an implantable battery-powered neurostimulator positioned subcutaneously in the abdominal wall [5].

stomach. Several animal and human studies with different GES settings support the efficacy of GES and alleviation of the symptoms [8], [9], [10], [11], [12], [13]. It has been found in [8] that for more than 95% of patients GES resulted in 80% reduction in vomiting and nausea.

2.4 Existing GES Treatment

The only available stimulator approved for humanitarian use by FDA for treatment of GP is a neurostimulator also known as Enterra therapy system [14]. The implanted GES system has two intramuscular electrodes (model no. 4300; Medtronic, Minneapolis) connected to the implanted neurostimulator. A pair of electrodes inserted by laparotomy or laparoscopy into the muscularis propria of the greater curvature, 10

cm from pylorus with electrode separation distance of 1 cm [5]. The neurostimulator is placed subcutaneously in the abdominal wall, as shown in fig. 2.2. The stimulator is programmed to a standard mode with certain parameters depending on the condition of the patient using a Medtronic (model no. 7432) programmer and a control software (model no. 7457). The average duration of the surgery is 1.6 hours. There are few postoperative cares required which include parenteral analgesia, sliding scale insulin administration in the diabetic patient, and jejunostomy feeding or conversion of parenteral nutrition to jejunostomy tube feedings [5].

2.5 Challenges

The existing device is battery operated, so it needs to be replaced every 3–6 years. The battery in the device contributes significantly to its size (5.5 cm $\times$ 6 cm $\times$ 1 cm). Thus a major surgery with a large incision is required to implant the stimulator. The device also uses a dedicated communication channel to change the device settings wirelessly causing an increase in the form factor of the device. Multiple replacement surgeries can be avoided by implementing a wirelessly powered gastric stimulator. It will also be beneficial to reduce the implant size so that it can be implanted by endoscopic procedures through mouth, throat, and esophagus into the stomach or minimally-invasive laparoscopy via a small incision in the abdomen. With these approaches, patients suffering could be minimized and a significant reduction in health-care costs can be achieved by eliminating hospital stay and repeated surgeries.

Although making a small implantable wirelessly powered gastric stimulator addresses the aforementioned issues, due to the rigidity of the device it could not conform to the stomach curvature. This presented an issue when stomach motility was resumed as the electrodes could not maintain a firm contact with the tissues for electrical current delivery. Additionally, over the time there exist chances of electrode malfunction due to stress generated on the electrodes for movement of the stomach.

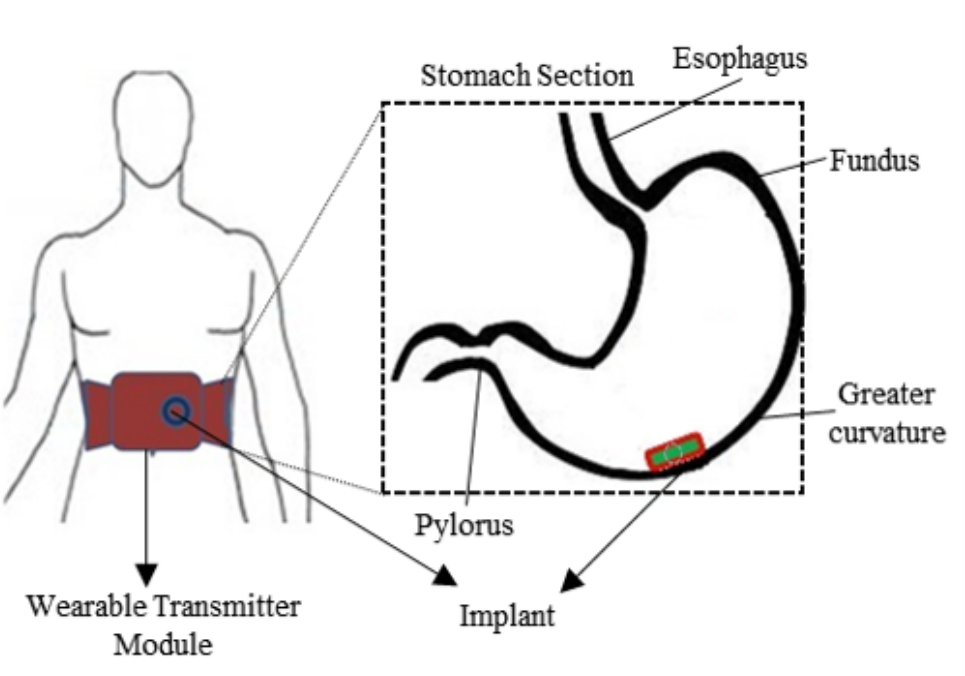

Fig. 2.3. Proposed implant configuration and wireless module.

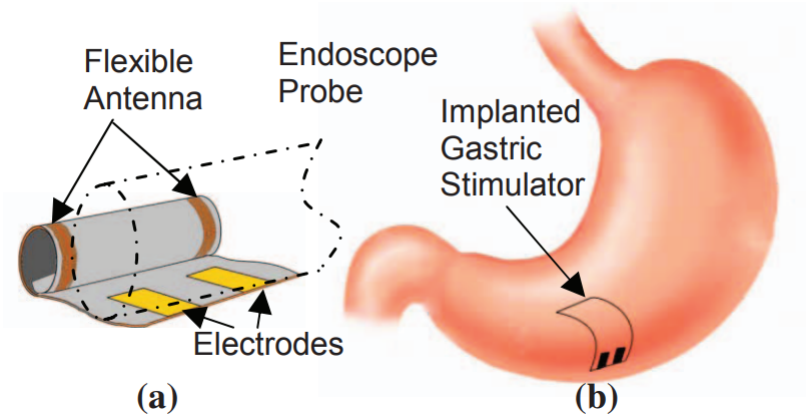

Fig. 2.4. The configuration of the flexible gastric stimulator. (a) The stimulator can be rolled into a capsule with a diameter of 7.95 mm. (b) Implanted gastric stimulator onto the stomach wall [15].

2.6 Proposed Application

A miniature implantable gastric stimulator was demonstrated in animal models previously by our group [16], [17]. The major objectives of this work are to minia-

turize the device and to introduce means to reconfigure the dosage settings without an additional communication link or adding another set of antennas. Wireless power transfer (WPT) to power medical implants is a promising alternative solution for volume consuming battery requirement in implantable devices. The WPT techniques have gained importance in various fields [18], [19], [20], [21], [22], however, the requirements for medical applications are very different from those for consumer appliances and industrial applications due to implant size, antenna size and shape, number of the electronic components and packaging constraints. To design an efficient WPT system for a miniaturized implant, certain parameters, such as implant configuration, device footprint, carrier frequency range for tissue barrier, power management and ergonomic design for implantation procedure and body motions, need to be taken into account.

In this work two miniaturized, wirelessly powered gastrostimulators with reconfigurable settings were demonstrated. The first stimulator design was rigid and powered with coil based energy harvesting antenna where as the second stimulator was flexible and rollable and powered by an monolithic spiral antenna. The transmitting coils were designed to fit comfortably around the abdominal area, without encompassing too large of an area. The gastrostimulator can be endoscopically implanted onto the wall inside the stomach, parallel to the abdominal muscle as seen in Fig. 2.3 and 2.4 for rigid and flexible stimulator respectively. Stimulation pulses can be delivered to the underlying tissues thorough attached electrodes.

3. SYSTEM DESIGN AND FABRICATION

3.1 Rigid Gastrostimulator

3.1.1 Wireless Power Transfer

Wireless power transfer using the near-field inductive coupling method has shown promising results to wirelessly-powered implantable medical devices [23], [24]. Inductive coupling WPT can be analyzed by basic electromagnetic theory since at low frequencies, quasi-static approximation can be applied as it has been assumed the fields are changing slowly in near field region [25]. The magnitude of the induced voltage in the receiver coil depends on the field distribution from the transmitting coil, medium between coils, size and shape of the coils, load impedance and the transmitted power.

Circuit Design

The WPT circuit was composed of three sections: an amplifier, tuning circuit, and the load. Figure 3.1 shows the simplified WPT circuit. A class-E amplifier circuit was used to generate sinusoidal signals at 1.3 MHz owing to the maximum possible exposure of human tissue to the electromagnetic field is highest in the band of 1.3–30 MHz [25]. The class-E amplifier circuit, chosen for its high efficiency, produced AC signals by switching Q_1, an N-channel power MOSFET (IRF510, Fairchild Semiconductor). A choke inductor L_D was used to block high-frequency signals and a shunt capacitor C_S was connected in parallel with the drain to source capacitance of the MOSFET to obtain zero-voltage switching class-E operation [26], [27]. A DC power supply V_D and a function generator V_S were used as power and signal sources, respectively. In the tuning circuits L_T and L_R representing the transmitting and receiving

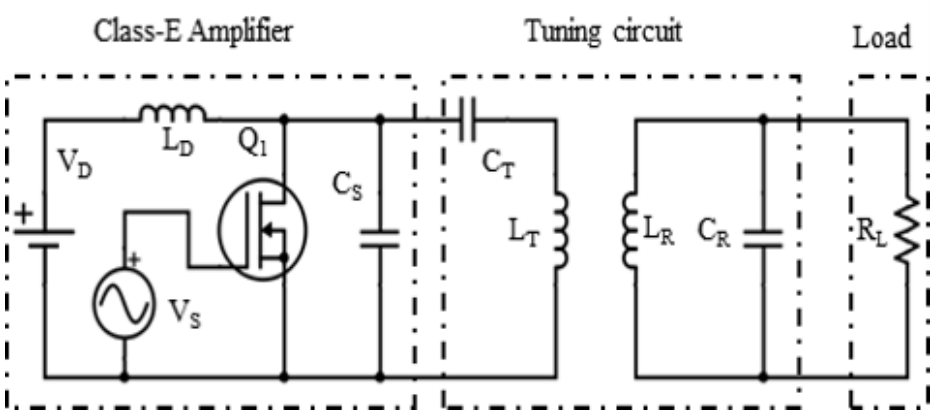

Fig. 3.1. Wireless power transfer circuit configuration.

coils, respectively, and C_T and C_R representing tuning capacitors. Both sets were initially tuned to resonance using the calculated capacitances. The configuration of the receiver bank determines whether the output of the wireless power circuit acts as a voltage (parallel configuration) or current source (series configuration). Since the digital circuitry requires a 5-V input voltage, the parallel configuration was chosen for the receiver [17]. A 500-Ω load resistor was used. In our previous work [17], a 500-Ω load was shown a good approximation of the stomach resistance for stimulating electrodes placed 1 cm apart. Once the circuit was constructed, the transmitting and receiving antennas were fixed at a distance, and then C_T and C_R were fine-tuned until a maximum power was received in the load.

Figure 3.2 shows a simplified circuit model used to analyze the system where R_1, L_1 and C_1 are the resistance, inductance and capacitance in the transmitter and R_2, L_2 and C_2 are for the receiver. R_3 is the load. M_{12} is the mutual inductance between the coils. I_1 and I_2 are the currents in the transmitter and receiver coil when V voltage is applied to the transmitter coil. Input power P_{in} and power delivered to the load P_{load} are

$$P_{in} = Re\{V\overline{I_1}\} \tag{3.1}$$

$$P_{load} = (\frac{I_2}{1 + j\omega R_3 C_2})^2 R_3 \tag{3.2}$$

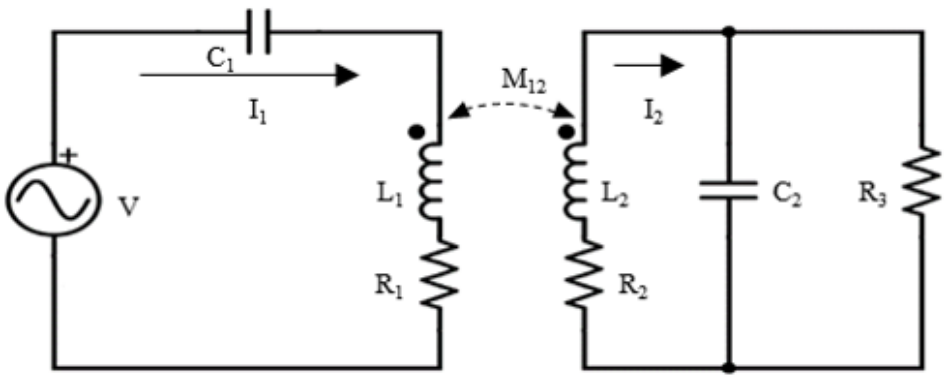

Fig. 3.2. Equivalent circuit model of the wireless power transfer system.

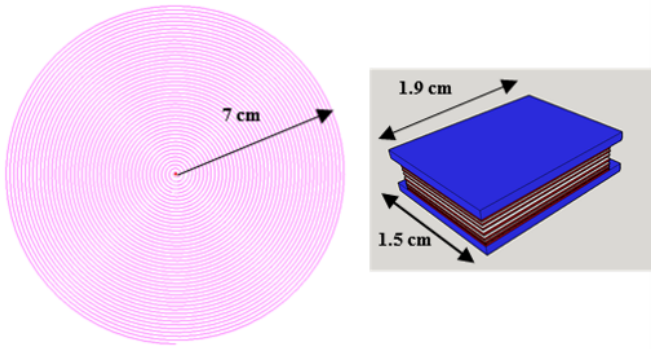

Fig. 3.3. Transmitter and receiver antennas.

Transmitting Antenna

Since the transmitting module will be worn on the abdomen, ensuring comfort for the user is a major factor in design. Size and flexibility of the antenna are taken into consideration for an ergonomic design. A spiral pattern was chosen over a radial pattern for the transmitting coil owing to better performance [27]. The coil width was limited to a radius of 7 cm to allow for average body types over the stomach, and 46/154 Litz wire was chosen for its flexibility and lower electrical resistance. A top view of the transmitting coil is in Fig. 3.3. The quality factor, inductance, and resistance of the coils were measured using an impedance analyzer (HP4192a).

Receiving Antenna

The receiving antennas were designed not to exceed 1.9 cm × 1.5 cm × 0.6 cm so that it could be placed inside the implant for endoscopic delivery. Owing to the small cross-section area of the receiving module, a radial pattern loop was chosen for the receiving antenna. This pattern improved turn-number efficiency over a small volume, which increased the self- and the mutual-inductance. The receiving coils were fabricated by winding wires around a 3D-printed polymer chassis. Care was taken for winding to ensure uniformity of the coils. The number of turns and different types of wires were investigated. Two different types of wires: 46/154 Litz and 24 gauge AWG wires were used to investigate 6, 8, 10, 12, 14, 16 and 18 turns coil antennas. The maximum number of turns was restricted to 18 due to the size constraints. The quality factor, resistance and inductance of the receiving coils were measured using the impedance analyzer, as shown in Tables 3.1 and 3.2.

Table 3.1.
Litz Wire Coil Parameters

Antenna	Tx_1	Rx_1	Rx_2	Rx_3	Rx_4	Rx_5	Rx_6	Rx_7
N	52	6	8	10	12	14	16	18
L(μH)	104	2.26	2.78	4.54	4.68	5.56	6.59	7.8
R(Ω)	18	2.61	2.77	3	3.03	3.29	3.49	3.77
Q	46.5	7.1	8.2	12.4	12.6	13.8	15.4	17

3.1.2 Implant

The stimulator consisted of energy harvesting circuitry and controller programmed with stimulator settings. The stimulator was made with a dual layer printed wiring board (PWB). After programming and testing the stimulator, the entire device is encapsulated in polydimethylsiloxane (PDMS). The electrodes from the stimulator

Table 3.2.
AWG Wire Coil Parameters

Antenna	Rx_8	Rx_9	Rx_{10}	Rx_{11}	Rx_{12}	Rx_{13}	Rx_{14}
N	6	8	10	12	14	16	18
L(μH)	2.32	2.98	4.14	4.35	5.66	6.22	6.61
R(Ω)	2.8	3.01	3.33	3.48	3.84	4.11	4.29
Q	6.8	8.1	10.1	10.2	12	12.4	12.6

can be clipped onto the walls of stomach. As shown in Fig. 3.4, AC to DC conversion was carried out in a bridge rectifier (CMKBR-6F, Central Semiconductor) with fast recovery characteristics and low quiescent loss. A low dropout linear voltage regulator (LM3480, Texas Instrument) was used to provide a regulated DC voltage to the next stage. The regulator was able to provide a maximum 100-mA current at an output voltage of 3.3 V with a 1-V dropout. The 1 μF capacitors (C_i and C_o) were introduced at the rectifier input and output stages to smooth out the rectified signal. 8-bit eXtreme Low Power (XLP) controller (PIC12lf1840, Microchip) with in-built flash memory was pre-programmed with different pulse settings. The controller has low power consumption and a small form factor with dual-flat no-leads (DFN) package. Signal was fed to the controller through a 10-kΩ feedback resistor R_f for frequency counting by which it was used for reconfiguration of pulse settings. The dual layer PWB had a dimensions of 1.3 cm $\times$ 0.72 cm. The implant after PDMS coating is shown in Fig. 3.5.

3.1.3 Remote Reconfiguration

Changing the pulse settings dynamically after device implantation adds options for gastroparesis treatment. In the existing treatment method [28], the pulse settings are changed using an active RF IC communication module with bi-directional wireless communication. Typical current consumption of the RF IC module is 12-20 mA [29].

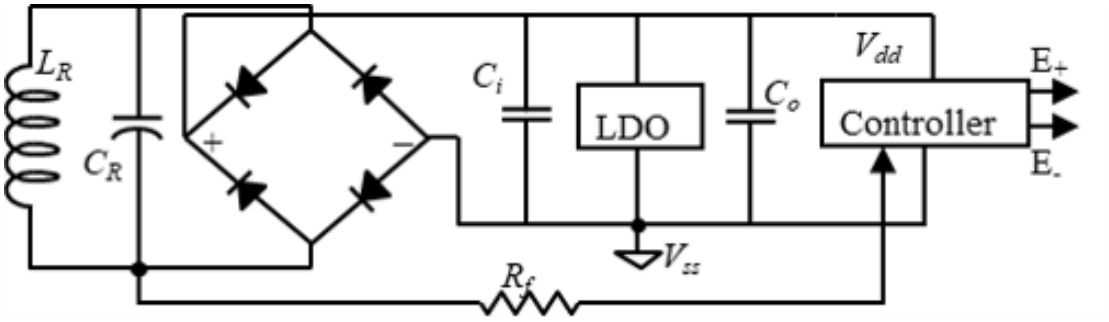

Fig. 3.4. Simplified stimulator circuit.

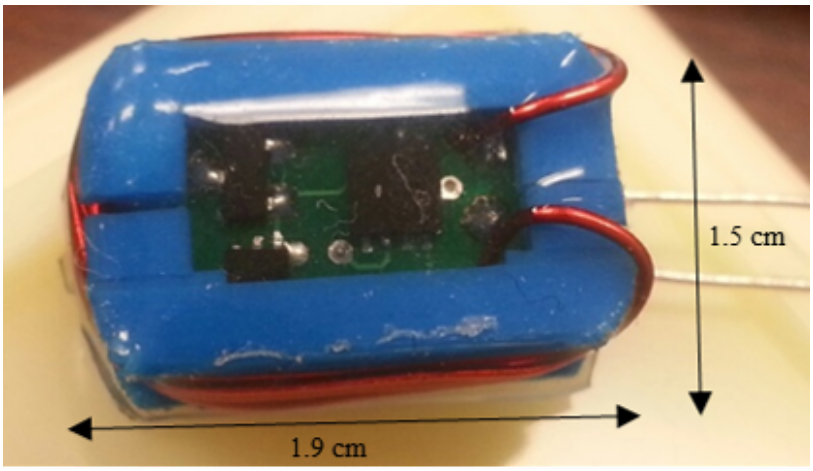

Fig. 3.5. The complete device with 3D printed groove to wind the receive coil antenna encapsulated in PDMS.

This method not only increases the form factor but also reduces battery life with more power consumption. A new method of remote reconfiguration was proposed by counting the incoming frequency of the power transfer carrier. The setting information is coded in the carrier frequency. With this approach, the aforementioned limitations can be addressed.

The bandwidth around the resonant frequency was sufficient to implement the remote reconfiguration algorithm. The available quality factor of the receiver LC circuit provided reasonable bandwidth. When the transmitted frequency was within

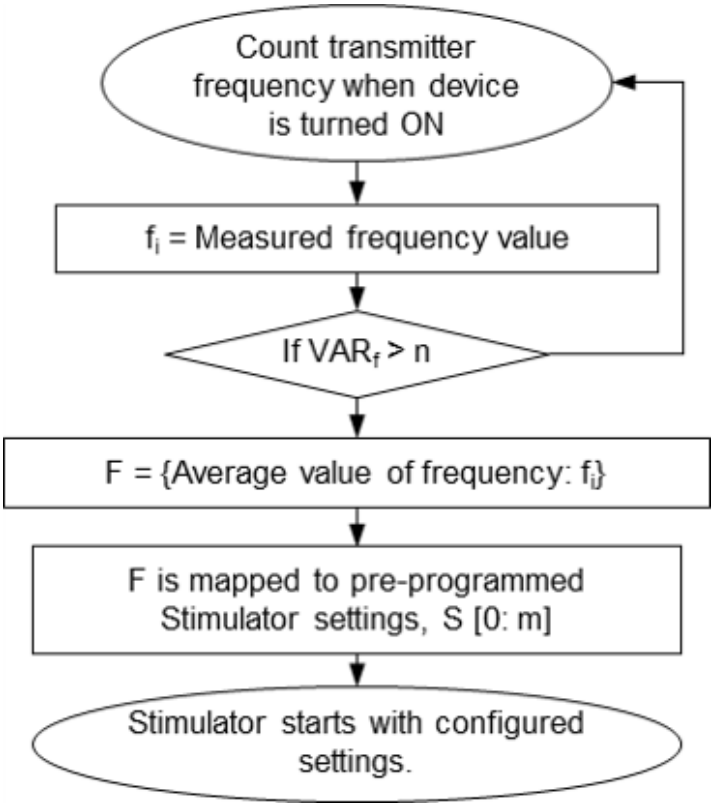

Fig. 3.6. Reconfiguration algorithm for mode changing of gastric stimulator.

the bandwidth Δf_{max}, the stimulator can be operated above the threshold power level. The entire bandwidth, Δf_{max} was divided into N_s, a maximum number of frequencies. The value of N_s could be calculated based on the resolution Δf_{min} which was the minimum separation between two frequencies which can be detected by the counter module present in the controller.

Internal oscillator of the controller was used as the reference clock for the timer to count the transmitting signal frequency. The logic flow in counting the frequency and changing the setting based on the input frequency is shown in Fig. 3.6. When the device was turned on, the frequency was counted n number of times and averaged for accuracy. The averaged frequency was then mapped to the stimulator settings stored in program memory of the microcontroller. Whenever the setting needed to be changed, the transmitter was turned off and the carrier frequency was changed to

the previously mapped value for the desired setting before the transmitter was turned on. The implant during boot-up read the new carrier frequency and started with the desired new settings.

3.2 Flexible Gastrostimulator

3.2.1 Concept

Figure 3.7(a) shows the conceptual drawing of the flexible gastric stimulator. The stimulator was fabricated on a flexible substrate, the electrodes and the stimulator circuit were designed on the one side of the substrate where as, the energy harvesting antenna was fabricated on the other side of the substrate. Owing to flexibility of the device it could be rolled into a cylinder-shape capsule to fit into the plastic tubing in the front end of an endoscope, is shown in Fig. 3.7(b). After the endoscope carries the stimulator into the stomach, a gripper through the working channel of the endoscope grabs the capsule and places it on the stomach wall. The stress of the flexible substrate opens the stimulator which returns to its flat condition. The device can be stapled onto the stomach tissues. Owing to the flexible nature, the substrate can conform to tissues and deform along with the stomach motion. Electromagnetic energy will be delivered from a transmitter antenna placed in belt which patient wears while eating. The flat stimulator consists of a coil to harvest inductively coupling energy, circuits to generate regulated stimulation pulses and electrodes in contact with tissues to deliver electrical currents. Stimulator will be turned on from outside the body while consuming food and it will provide stimulation dosage as set by doctor.

3.2.2 Transmitter Antenna

The transmitter antenna was designed considering the coverage area and efficiency of WPT at resonant frequency. Ensuring comfort for the patient is another major factor in choosing the size of the antenna since the transmitting module will be worn

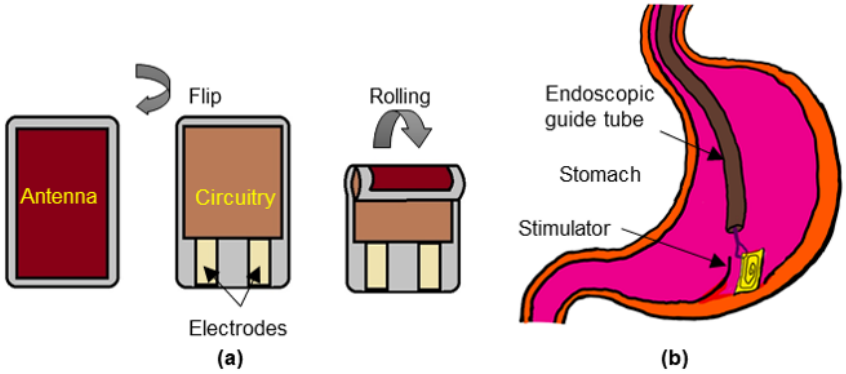

Fig. 3.7. (a) The conceptual drawing of flexible gastric stimulator and (b) placement of the flexible gastrostimulator in submucosal layer by endoscopic process.

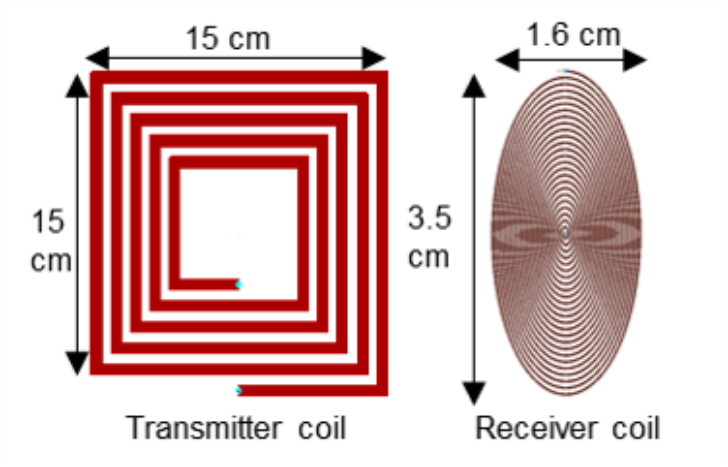

Fig. 3.8. Transmitter and receiver antenna designs of the flexible gastrostimulator.

on the abdomen during treatment. A 15 cm × 15 cm rectangular spiral antenna was chosen over a radial pattern for the transmitting coil owing to better performance [27]. The transmitter antenna was fabricated by photolithography and wet etching of copper coated flame retardant (FR4) board.

3.2.3 Receiver Antenna

The receiving antenna was designed not to exceed 3 cm × 1.6 cm so that it could be rolled and placed inside the guide tube for endoscopic delivery. An elliptical planar spiral antenna was fabricated using photolithography and wet copper etching on the one side of the 25.4-μm flexible polyimide substrate. The number of turns and spacing were optimized for a higher quality factor of the antenna while maintaining the flexibility of the implant device. A top view of the transmitting and receiving coil is in Fig. 3.8. The quality factor, inductance and resistance of the coils were measured using an impedance analyzer (HP4192a) and given in table 3.3.

Table 3.3.
Transmitter and Receiver Antenna Parameters

Parameters	**Transmitter**	**Receiver**
Shape	Rectangular spiral	Elliptical spiral
Substrate	FR4	Kapton(25.4 μm)
Length	15 cm	3.5 cm
Width	15 cm	1.6 cm
Number of turns	5	25
Line width	5 mm	12 μm
Line spacing	5 mm	60 μm
Copper thickness	35 μm	12 μm
Inductance	3.44 μH	6.79 μH
Resistance	1.7 Ω	19.6 Ω
Quality factor	86	15

3.2.4 Transmitter Circuit Design

There were three primary sections in the WPT system; an amplifier, tuning circuit and the load. The simplified WPT circuit is shown in Fig. 3.9. A highly efficient class-E amplifier circuit was used to generate sinusoidal signals at 6.78 MHz. The class-E amplifier circuit, chosen for its high efficiency [30], produced AC signals by switching

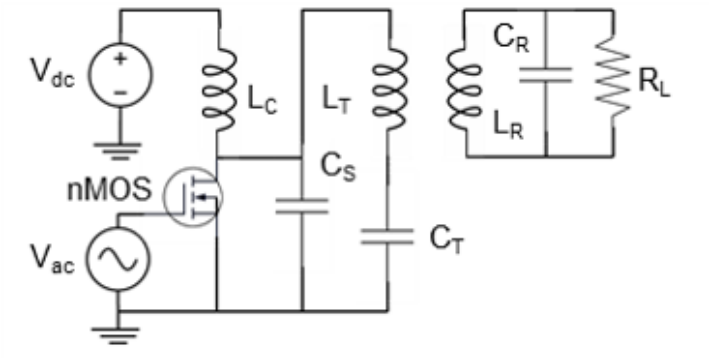

Fig. 3.9. Transmitter circuit diagram of the WPT system designed for flexible gastric stimulator.

a N-channel power MOSFET (IRF510, Fairchild Semiconductor). A choke inductor L_C was used to block high-frequency signals and a shunt capacitor C_S was connected in parallel with the drain to source capacitance of the MOSFET to obtain zero-voltage switching class-E operation [26], [27]. A DC power supply V_{dc} and a function generator V_{ac} were used as power and signal sources, respectively. In the tuning circuits L_T and L_R represent the transmitting and receiving coils, respectively, and C_T and C_R represent tuning capacitors. Initially, the transmitter and receiver coils were tuned to resonance using the calculated capacitances. A 500-Ω load resistance R_L was used for WPT system characterization as it was shown a good approximation of the stomach resistance for stimulating electrodes placed 1 cm apart in our previous work [17].

3.2.5 Implant

In order to design the flexible gastric stimulator as conceptualized in the previous section, there were several parameters which were required optimization. Since the device was required to operate without a battery, energy harvesting antenna was one of the crucial parameters. With thicker copper deposition and increased number of turns the quality factor of the antenna could be increased, however, it would be

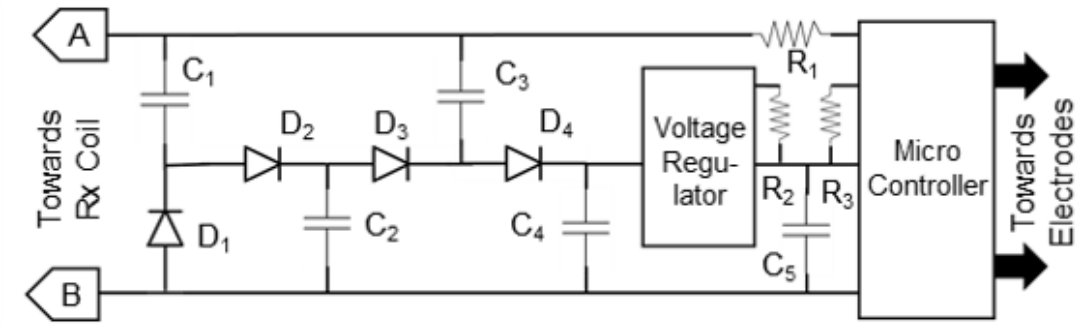

Fig. 3.10. Simplified circuit diagram of the flexible gastric stimulator.

extremely difficult to etch high aspect ratio structures on the film. Even though, if the etching issue was dealt the flexibility of the device would be compromised if the copper thickness was not optimized. The receiver circuit was also designed carefully, by considering the number and placement of the active and passive components in the circuit. All these aspects of the implant are discussed below with their merits and constraints.

Implant Circuit Design

Figure 3.10 shows the circuit diagram of the flexible gastrostimulator. The receiver coil was tuned to resonate at 6.78 MHz by a parallel capacitance and the connected to the ends marked A and B in the circuit diagram. Unlike rigid gastrostimulator, a two stage charge pump circuit was used to convert AC signal to DC and boost the energy harvesting voltage so that it could be used by micro-controller. It was expected that the power harvesting performance using the flexible antenna would be much less in comparison to the rigid gastrostimulator antenna due the quality factor of the receiver antenna. The use of charge pump circuit was able to resolve the problem of generating adequate voltage to run the digital circuitry. In spite of the trade off of producing a lower current(around 10 mA) with charge pump circuit, it was sufficient for gastrostimulator application. A 50-mA low drop out voltage reg-

ulator (TPS79733DCKR, Texas Instruments) was used after the charge pump stage for maintaining the input voltage to the micro-controller to 3.3 V. Like rigid stimulator, a 8-bit eXtreme Low Power (XLP) controller (PIC12lf1840, Microchip) with in-built flash memory was pre-programmed to provide required stimulation pulses and to perform mode changes based on the communication protocol discussed earlier. The resistor R_1 fed the frequency information used for communication with the transmitter. The circuit parameter values for flexible gastric stimulator are given in table 3.4.

Table 3.4.
Flexible Gastrostimulator Circuit Parameters

Parameters	**Details**
C_1,C_2,C_3	20 nF
C_4	1 μF
C_5	10 μF
D_1,D_2,D_3,D_3	SMS7630-061 Schottky diode from Skyworks
R_1	10$k\Omega$
R_2	100$k\Omega$
R_3	10$k\Omega$

Fabrication

The flexible stimulator was fabricated using double side copper coated polyimide substrate (Pyralux AP7163E, Dupont) [31]. The thickness of the copper and polyimide were 12 μm and 25.4 μm respectively. The copper used in this substrate was known as wrought copper and it was produced by heating and mechanically rolling ingots of pure copper to a desired thickness through rollers. Unlike sputtering or e-beam deposition this process produces copper with a grain structure that resembles overlapping plates and the structure has significantly longer crack propagation path

and provides a copper film with a higher tensile strength . Thus, this substrate was chosen for flexible gastrostimulator design.

Table 3.5.
Photolithography Recipe

Parameters	**Details**
Photoresist	NR9-1500PY, Futurrex
Spin coating	3000 RPM for 30 sec
Resist thickness	1.5 μm
Pre bake time	2 min at 150^{o}C sec
Exposure time	14 sec
Post bake time	5 min at 100^{o}C sec
Developer	RD6
Development time	10 sec

Figure 3.11 shows the complete fabrication process and it had 13 steps. The film was cleaned with isopropyl alcohol(IPA). After cleaning the film was attached to a 130 mm silicon wafer using a Kapton tape and coated with NR9-1500PY photoresist and then exposed to UV light through a chrome mask. The circuit patterns were developed using RD-6 developer. Table 3.5 summarizes the photolithography parameters. Once the circuit side of the substrate was patterned, the antenna side of the sample was protected using a Kapton tape and top layer of the copper was etched using Copper Etchant CE-100 (Transene Company, Inc.). After fabricating the circuit patterns, the sample was cleaned with de-ionized (DI) water and residue resist was removed using acetone. Next, the antenna side was exposed and the circuit side was protected using the Kapton tape and the entire process was repeated to obtain the antenna pattern on the other side of the substrate. Finally, the device was cleaned with DI water and acetone and shown in Fig. 3.12. All active and passive circuit components were soldered to the fabricated device using a low-temperature lead-free solder paste (SSLTNC-15G, SRA Soldering Products) and reflow soldering machine. Unlike other

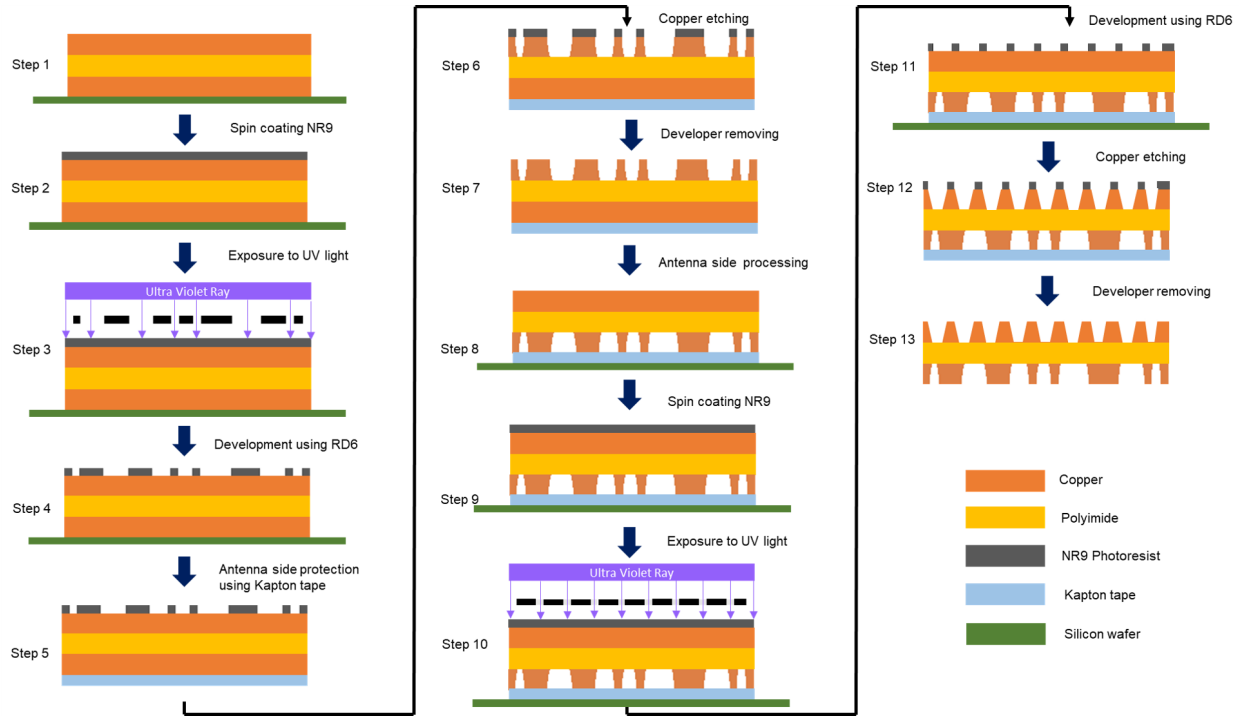

Fig. 3.11. Fabrication process of the flexible gastric stimulator.

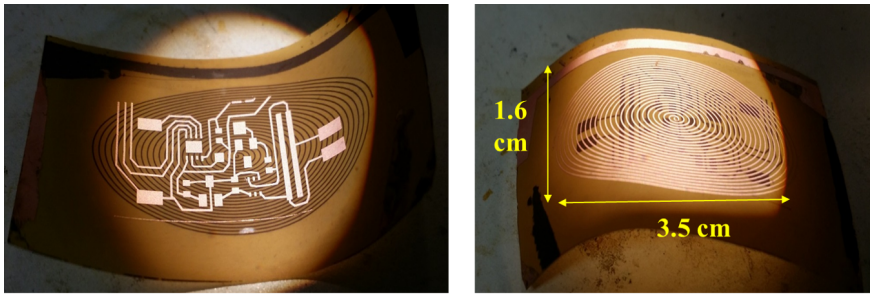

Fig. 3.12. The fabricated gastrostimulator with antenna and circuit on either side of the flexible substrate.

active components, the micro-controller was programmed on separate board and then soldered to the flexible gastrostimulator.

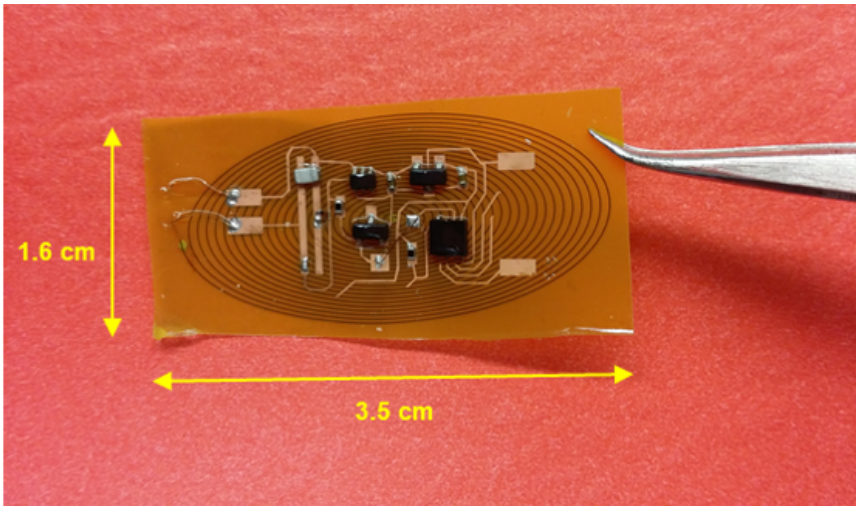

Fig. 3.13. The flexible gastrostimulator encapsulated with PDMS.

Encapsulation

Since the device will be implanted inside a human body, it was required to be encapsulated using bio-compatible substrate. The polydimethylsiloxane (PDMS) is widely used bio-compatible material for encapsulation of medical implants [32], [33]. Like rigid gastrostimulator flexible gastrostimulator was also dip coated with PDMS and cured at room temperature over 2 days of duration. The PDMS layer not only provided the encapsulation to the device, it also provided the stress to open up from rolled state to unroll state when released from the endoscope guide tube. The electrodes of the stimulator were exposed by removing the PDMS encapsulation on top of it. Figure 3.13 and 3.14 show the fabricated flexible gastric stimulator with PDMS encapsulation and Fig. 3.15 shows that the gastrostimulator was rolled and placed in a cylindrical tube to demonstrate the feasibility of the endoscopic implantation.

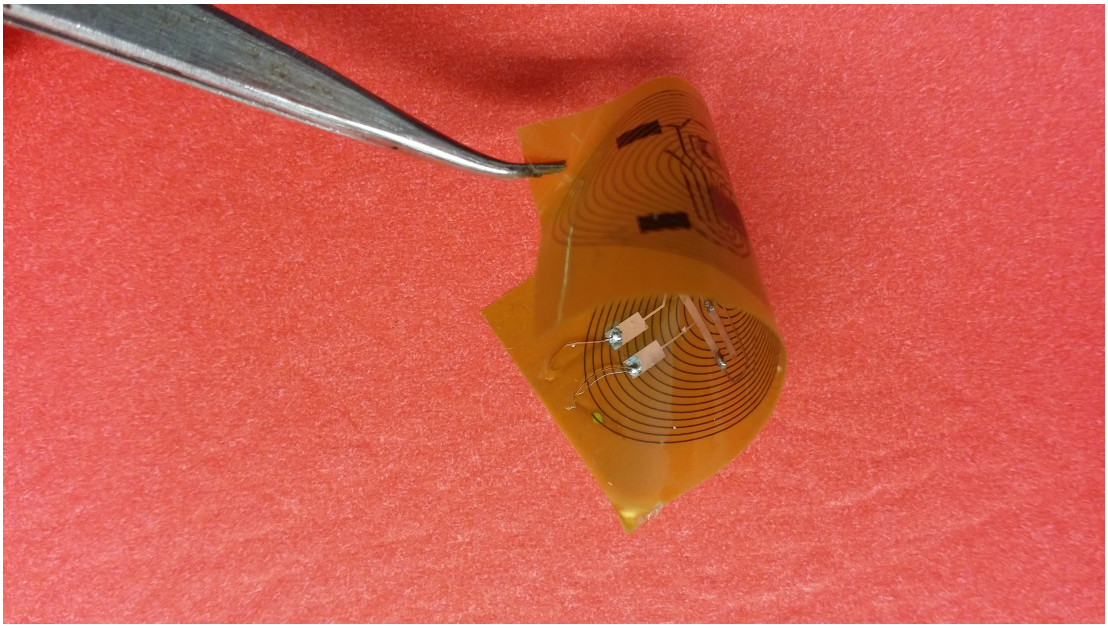

Fig. 3.14. Flexibility testing of the flexible gastrostimulator.

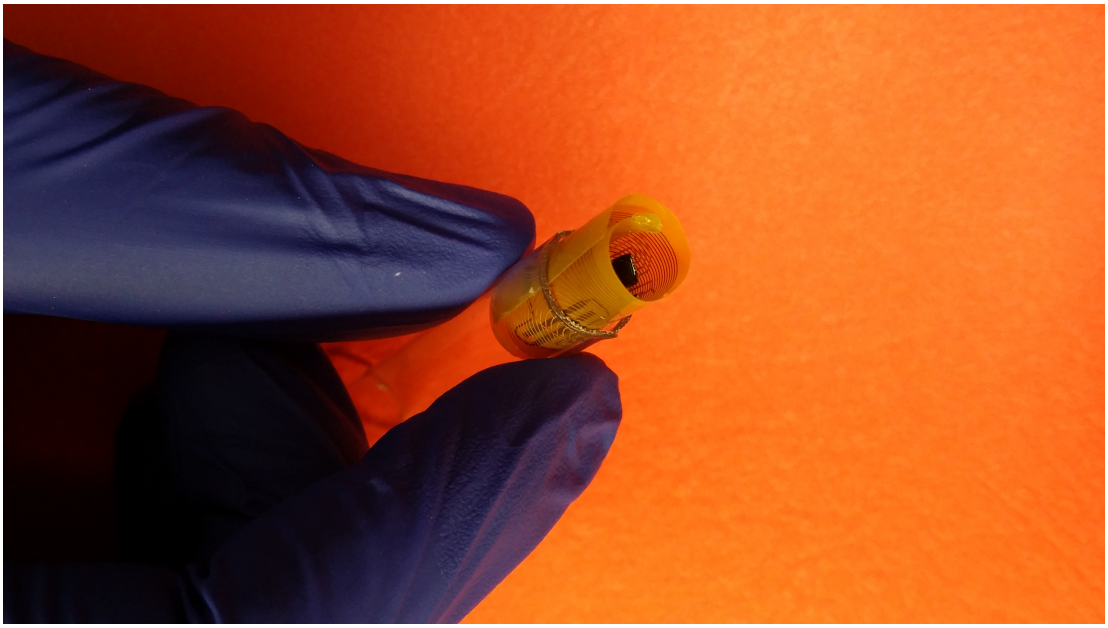

Fig. 3.15. The flexible gastrostimulator rolled and placed in a cylindrical tube to demonstrate feasibility of the endoscopic implantation.

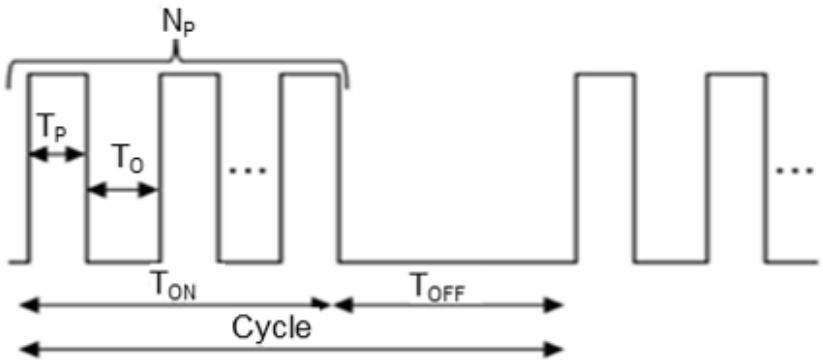

Fig. 3.16. Typical stimulation cycle.

3.3 Stimulation Parameter

The stimulator pulse requirements were obtained from previous animal work [17], and a typical stimulation signal cycle is shown in Fig. 3.16. Initially, the controller was programmed with a pulse width T_p of 330 μs with a frequency of 14 Hz. This sequence is ON for 0.1 s and OFF for 5 s. N_p is the number of pulses within the ON sequence. The stimulator pulse settings can be reconfigured remotely based on the patients needs after implantation. The change of dosage setting in actual treatments is guided by various parameters such as mean weekly patient vomiting frequency, symptom severity and gastric emptying [34]. Table 3.6 summarizes three different dosage levels typically used in the treatment.

Table 3.6.
Pulse Train Specification For Gastric Stimulation

Settings	T_p	T_o	T_{on}	T_{off}	N_p
Low	330μs	14 Hz/71.4 ms	0.1 s	5 s	2
Medium	330μs	28 Hz/35.7 ms	1 s	4 s	30
High	330μs	55 Hz//18.2 ms	4 s	1 s	220

4. EXPERIMENTS AND CHARACTERIZATION

4.1 Rigid Gastrostimulator

4.1.1 Wireless Power Transfer

Benchtop studies were performed to determine the effects of distance and number of coil turns on the power transfer. 5-V square waveforms with a 50% duty cycle at 1.3 MHz drove the amplifier. A 500-Ω resistor was used as the load. Each receiving coil was tested individually. The power received was calculated by,

$$P_r = \frac{V_{Lrms}^2}{R_L} \tag{4.1}$$

V_{Lrms} is the root mean square (rms) voltage across the load. The wireless power transfer efficiency was obtained by,

$$\eta_{eff} = \frac{P_{out}}{P_{in}} = \frac{P_r}{V_{dd} \times I_{dd}} \tag{4.2}$$

V_{dd} and I_{dd} are the DC input voltage and current, respectively, on the transmitting circuit. Initially the transmitter and receiver circuits were tuned at a distance of 4 cm for maximum received power at 1.3 MHz. Parasitic capacitance adjustment was needed to fine-tune the circuits until a maximum power was recorded on the load. A set of experiments were carried out to investigate the system performance.

Effect of Distance

The experimental setup for antenna characterization is shown in Fig. 4.1. Transmitting coil was kept stationary with the receiving coil moving at a step of 1 cm in a range of 1–10 cm, with the centers of the antennas aligned to each other. The experiments were carried out using two sets of receiver antennas made of AWG-24 gauge

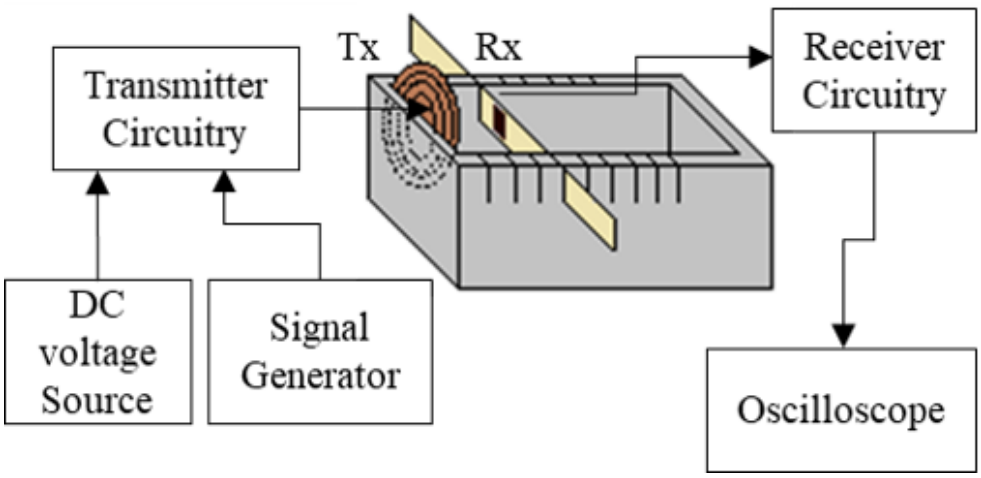

Fig. 4.1. Experimental setup diagram for wireless power transfer with rigid gastrostimulator.

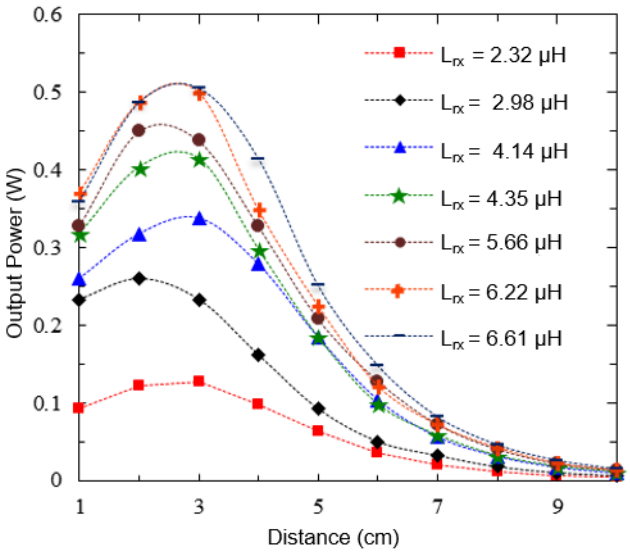

Fig. 4.2. Power received by the AWG wire receiver antennas at various distances.

wires and Litz wires. Figure 4.2 shows power received by the AWG coil antennas with various inductances at different distances. Maximum power was 510 mW for the distance range of 2–4 cm for the receiver with an inductance of 6.61 μH. With

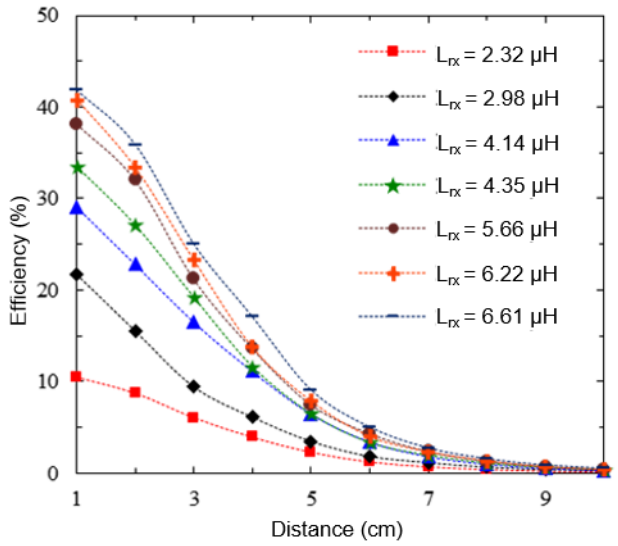

Fig. 4.3. Power transfer efficiencies of the AWG wire receiver antennas at various distances.

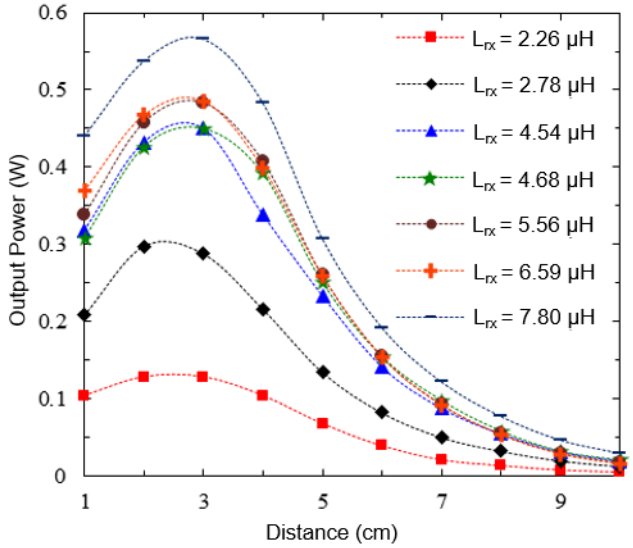

Fig. 4.4. Power received by the Litz wire receiver antennas at various distances.

the same inductance, the maximum efficiency was 42% at the 1-cm separation and efficiencies above 17.1% were maintained for distances up to 4 cm as shown in Fig.

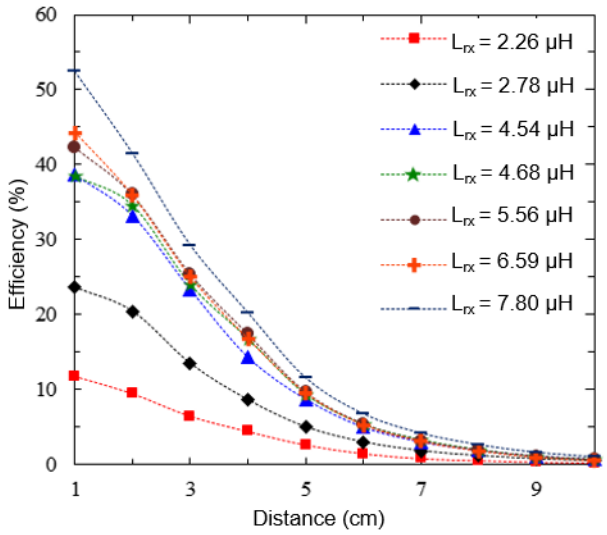

Fig. 4.5. Power transfer efficiencies of the Litz wire receiver antennas at various distances.

4.3. Figures 4.4 and 4.5 show the output power received and power transfer efficiency using Litz wire antennas. A maximum power of 570 mW was observed using Litz wire antenna of 7.8 μH, with 11.8% improvement over the AWG wire antenna of 6.61 μH, for the distance range of 2–4 cm. The power transfer efficiency at 4 cm improved to 20.2%. The results were expected since the quality factors of Litz wire coils were higher compared to AWG ones as shown in Tables 3.1 and 3.2. Owing to better performance, the Litz wire antenna with 7.8 μH was chosen for further investigations. The mutual inductance M between the transmitter and receiver was obtained with the open- and short-circuit method [35] as

$$M = (\sqrt{1 - \frac{Z_{short}}{Z_{open}}})(\sqrt{L_{Tx}L_{Rx}}) \tag{4.3}$$

where Z_{open} and Z_{short} were the measured impedances of the transmitter coil with the receiver coil kept open or shorted. The L_{Tx} and L_{Rx} are the measured self-inductances of the transmitter and receiver coils, given in Tables 3.1 and 3.2. The transfer power and efficiency were calculated using the measured mutual inductances

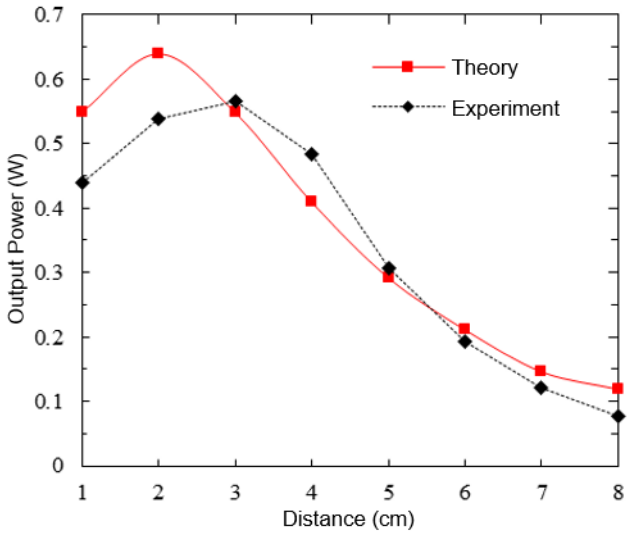

Fig. 4.6. Comparison of output powers received at various distances in air.

in the equivalent circuit model. The comparison results are shown in Figs. 4.6 and 4.7. The measured results matched with the theoretical ones. However at very short distances, owing to strong mutual coupling between the coils, the input impedance of the equivalent circuit in the transmitter changed, which contributed impedance mismatch in the class-E amplifier reducing the output power. In spite of the drop in output power for the distance range less than 3 cm, the efficiency did not decrease. This phenomenon was due to that the change in the input impedance also caused input power to drop.

The frequency responses of the WPT system are shown in Figs. 4.8 and 4.9. The WPT system was tuned to 1.3 MHz at every distance of measurement and the input frequency varied in the range of 1.2–1.55 MHz. The half power bandwidth of the system was measured by calculating the half power point in Fig. 4.8. The half power bandwidth was 10-kHz for a 4-cm antenna separation distance in air. This bandwidth information was helpful for designing the wireless communication algorithm between transmitter and receiver. Figure 4.9 shows stable power transfer efficiencies over the frequency range of 1.29–1.4 MHz for different distances in air.

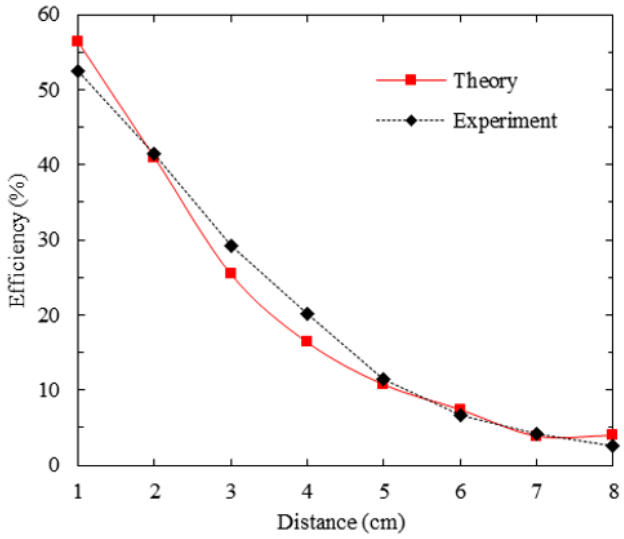

Fig. 4.7. Comparison of WPT efficiencies at various distances in air.

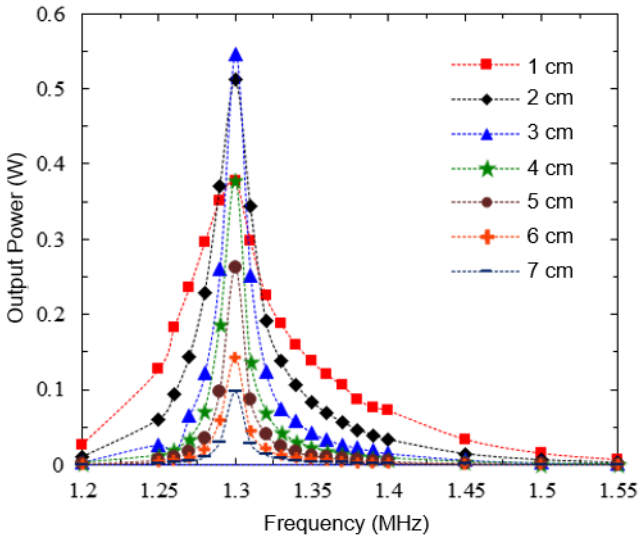

Fig. 4.8. Output powers received at various distances as a function of frequency.

Effect of Misalignment

In practical scenarios the implant will not be perfectly aligned to the transmitter antenna owing to various factors like stomach movements, placement of the device

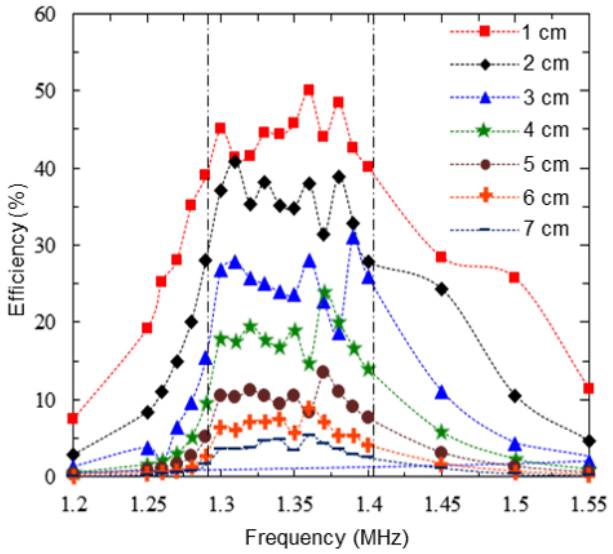

Fig. 4.9. Power transfer efficiencies of receiver at various distances as function of frequency.

during surgery and the fact that the patients do not know the exact location before they put on the belt every morning. It is important to study the power transfer effect from misalignment. Linear and angular misalignment effects were studied to determine the performances at different distances. The receiving and transmitting antennas were fixed at a 4-cm spacing and system was tuned to the resonant frequency. For linear misalignment studies, the transmitter antenna was kept fixed and receiver antenna was moved in the cross section plane facing the transmitter at a 4-cm distance. The receiver antenna was moved along the x-, y-and 45^o-axis in the cross section plane. Shown in Fig. 4.10, 60% of the maximum output power, which was the power received with perfect center-to-center alignment, was maintained within a 6-cm diameter area. The field pattern from the transmitting antenna was symmetrical. The same experiments were repeated, with the coil tuned for the 4-cm spacing distance, for different spacing distance without re-tuning the transmitting coil. This is assuming that once the care-giver helps the patient to optimize the antenna setting,

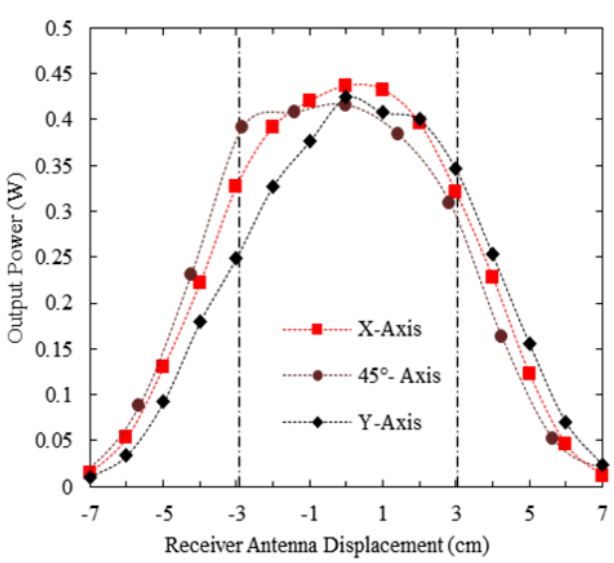

Fig. 4.10. Output powers as a function of misalignment.

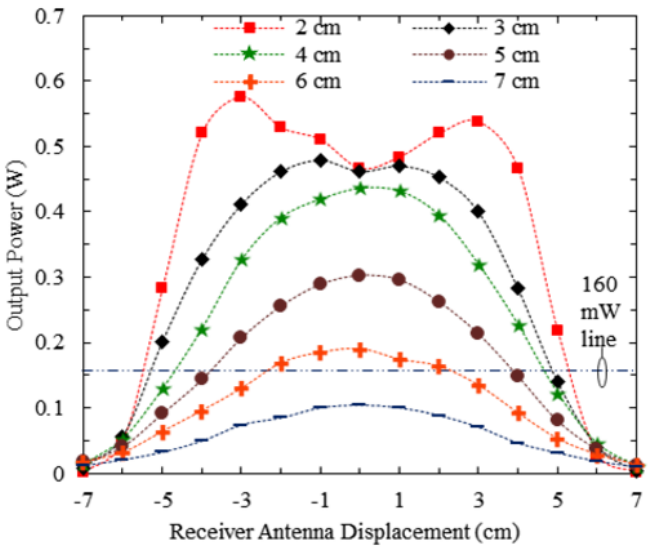

Fig. 4.11. Output power variation for due to misalignment at various distances.

the tuning capacitance is fixed. The received power and transfer efficiency at different locations along the x axis are shown in Figs. 4.11 and 4.12, respectively.

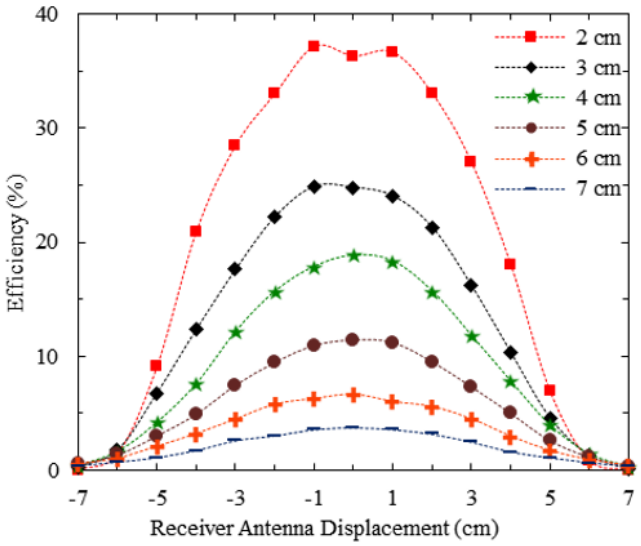

Fig. 4.12. Efficiency variation for due to misalignment at various distances.

The drop in power at the perfect alignment condition (zero on the location axis) for the 2-cm coil separation, as shown in Fig. 4.11, was due to the additional mutual inductance that affected the amplifier impedance and tuned the system out of resonance because the system was first tuned for the distance of 4 cm. However, the efficiency shown in Fig. 4.12, did not drop at 2 cm when the coils were aligned center-to-center. This was due to the input power also decreased, while the output power decreased, resulted by the de-tuned transmitter circuit. As the gastric stimulator required at least 160 mW in power to deliver sufficient energy to the tissues, the system can tolerate misalignment within diameters of 11.0, 10.1, 9.2, 7.1 and 4.0 cm for 2, 3, 4, 5 and 6 cm of antenna separations, respectively.

The magnetic field coupling between the transmitting and receiving antennas depends on the orientation of the receiving antenna. As the relative angular orientation changes, the receiving coil couples both normal and tangential components of the magnetic fields. Therefore, the total harvested energy depends on the relative location for coils that are not perfectly in parallel. At the center-to-center alignment,

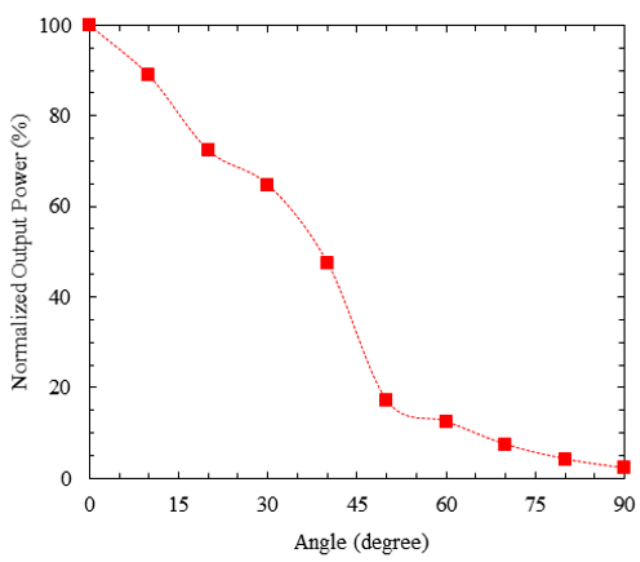

Fig. 4.13. Output power variation with angular misalignment at 4 cm.

the receiving coil, since it is much smaller than the transmitting antenna, receives only the normal component of fields. Figure 4.13 shows a decrease of received power, normalized to maximum power received at a 4-cm separation, as the receiving antenna rotated at intervals of 10^o until the receiving antenna was perpendicular with the transmitting coil. The received power matched theoretical prediction. Ideally the received power should have reached zero, but some tangential component of field was coupled.

Effect of Dielectric Layers

The presence of tissues between the coils was expected to have an effect on the power transfer due to dielectric properties changing the mutual inductance and parasitic capacitance. It results resonant frequency shifts beside conductive losses. Literatures suggested 0.9% saline and pork slices to mimic human body tissues [36], [37], [38]. They were both studied for effects in loss and resonance frequency.

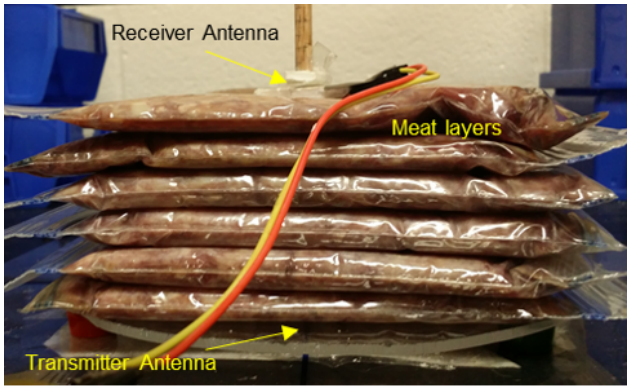

Fig. 4.14. Photo of experimental setup for meat experiment.

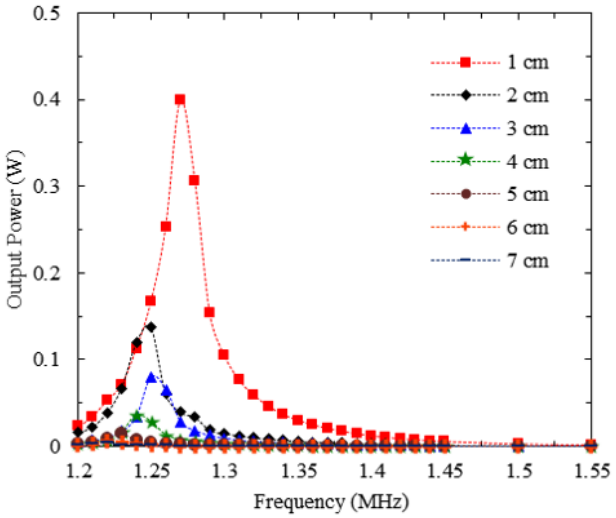

Fig. 4.15. Output power variation in presence meat at various distances (without tuning).

The experiments were conducted by placing these dielectric materials between coils. The pork, moist with phosphate buffered saline, and saline were kept in 15 cm × 15 cm × 1 cm plastic bags which could be stacked for various thicknesses as shown in Fig. 4.14. Once both the transmitting and receiving circuits were tuned to the resonance at the spacing of 4 cm in air, spacing distances were varied with bags

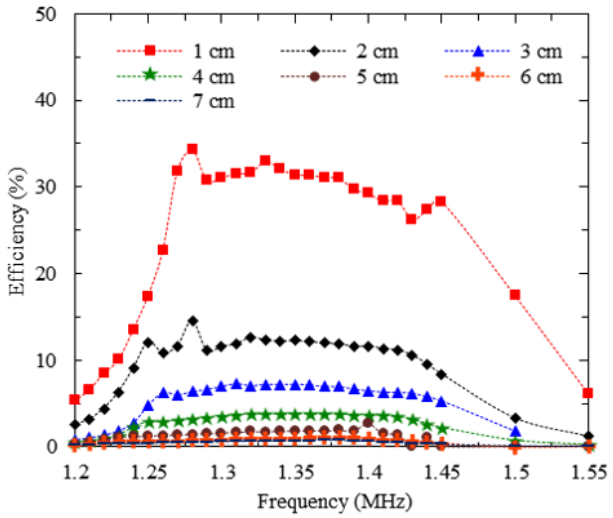

Fig. 4.16. WPT efficiencies at various distances in presence of meat (without tuning).

inserted. Resonance frequency shifts were observed. Then the transmitting circuit was re-tuned back to 1.3 MHz to increase power at the load until it reached maximum.

Figure 4.15 shows output power at the receiver with various thicknesses of pork. Peak frequencies shifted 30, 50, 55 and 60 kHz for 1, 2, 3 and 4 cm slice thicknesses, respectively. The maximum output power through 4-cm pork slice was 36 mW, reduced by 342 mW when compared to the maximum output power through 4-cm air (378-mW) as shown in Fig. 4.8. The power transfer efficiencies were also measured and shown in Fig. 4.16. An efficiency of 30% was maintained over the frequency range of 1.25–1.45 MHz for 1-cm thick pork while it dropped to 3.44% for the 4-cm thick pork, compared to results in air (18.5%) shown in Fig. 4.9. In practical scenarios, only the transmitter coil and circuit can be re-tuned after implantation. Therefore, with the existence of pork tissues, the transmitter was re-tuned to regain the power. Figures 4.17 and 4.18 show the output powers and efficiencies when the transmitting circuit capacitor was re-tuned to operate at 1.3 MHz. As shown in Fig. 4.17, the

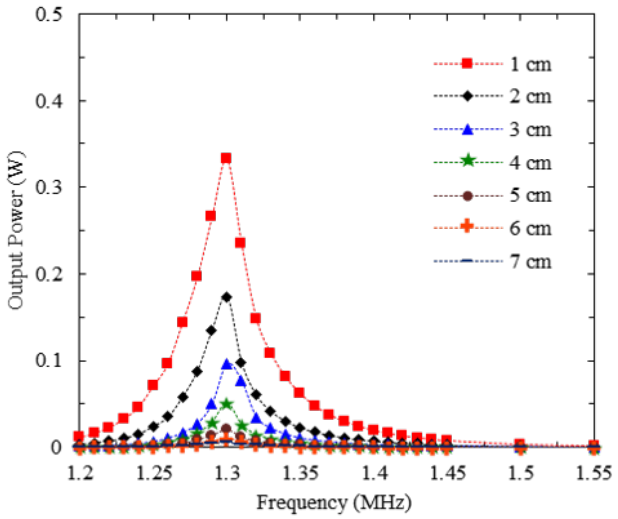

Fig. 4.17. Output power variation in presence of meat at various distances with re-tuning (system was re-tuned to 1.3 MHz after placing the pork slices).

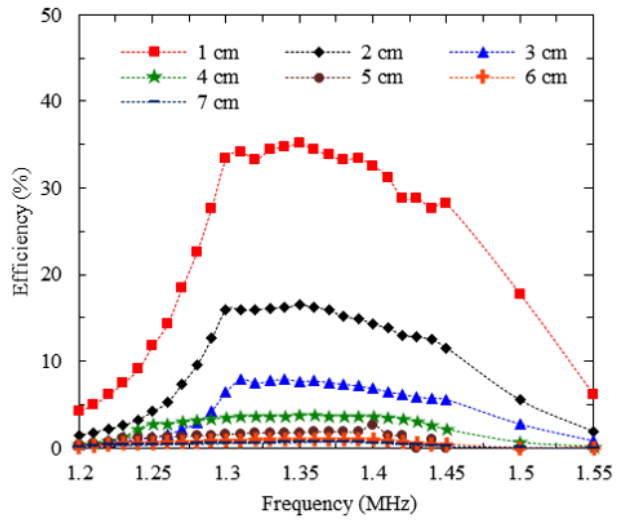

Fig. 4.18. WPT efficiencies at various distances in presence of meat (system was re-tuned to 1.3 MHz after placing the pork slices).

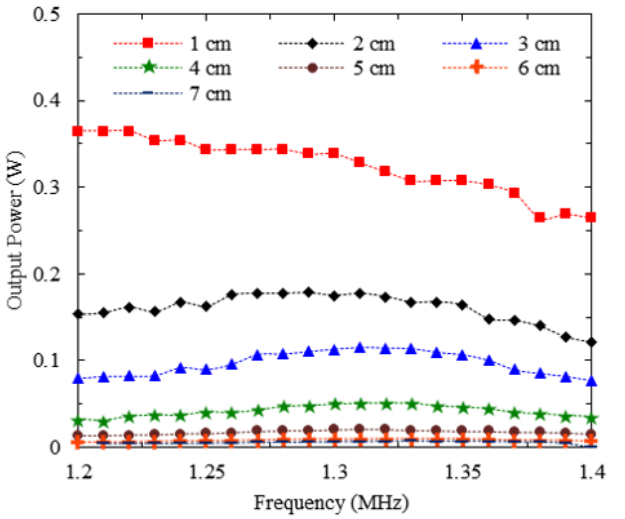

Fig. 4.19. Output power variation in presence of meat at various distances with re-tuning (system was re-tuned to the corresponding measurement frequencies after placing the pork slices).

output powers reached maximum at 1.3 MHz for all different thicknesses of pork. The maximum output power for 4-cm thickness was 51 mW which was 22 mW higher than the untuned result shown in Fig. 4.15. Similarly, the transfer efficiencies were maintained over frequency ranges around 1.3 MHz, 3.7% efficiency was observed at 4 cm as shown in Fig. 4.18.

Another set of experiments was carried out by swiping the input frequency in 1.2–1.55 MHz band with a step of 10 kHz and re-tuning the transmitting circuit at every step. This experiment helped to identify the bandwidth available for reconfiguration of the gastric stimulator as explained in system design section. Figures 4.19 and 4.20 show the results by re-tuning each frequency within the 0.35-MHz bandwidth. The output powers at the receiver were maintained within ± 2.62% of the power received at 1.3 MHz for 1-cm tissue thickness whereas they were maintained within ± 0.83% of the power received at 1.3 MHz for 4-cm thickness. Similarly shown in Fig. 4.20,

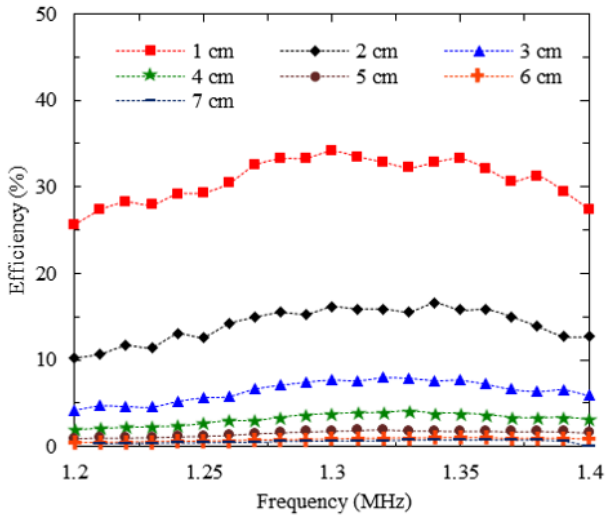

Fig. 4.20. WPT efficiencies at various distances in presence of meat with re-tuning (system was re-tuned to the corresponding measurement frequencies after placing the pork slices).

power transfer efficiencies were maintained within ± 3.33% and ± 0.66% for 1-cm and 4-cm thick pork, respectively.

Table 4.1 summarizes the changes in quality factor before and after re-turning the transmitting capacitance for pork of various thicknesses. The changes in the quality factor indicate that re-tuning of the transmitter add additional losses due to impedance mismatch between transmitter circuit and the transmitter coil. The power transfer experiments were repeated with saline to compare and the results are shown in Fig. 4.21. The WPT system had a higher efficiency and power transferred in air than in saline or meat, as expected, due to the ionic losses in the saline and pork. The efficiencies were similar when both pork and saline were placed between the coils, at 4-cm separation efficiencies dropped by 15.3% and 16.47% for saline and pork, respectively. In air with short distance, the high mutual inductance from strong coupling affects the input impedance of the transmitter coil and reduce the transferred output power at the receiver. The input power to the amplifier however

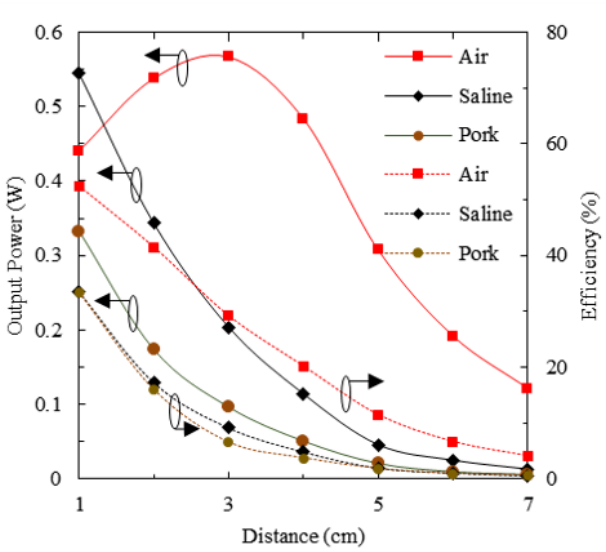

Fig. 4.21. Comparison of output power and efficiency at different thicknesses of dielectric mediums.

varies accordingly so the efficiency remains high. This phenomenon did not apply for saline or pork because the parasitic capacitances from the dielectric materials altered the resonant frequency of the coils away from the operating frequency so the coupling is not as strong at the near distance. Although the transmitter coil could be re-tuned back to the operating frequency, the receiver was still off the resonance.

Table 4.1.
Quality Factor of the WPT System

Thickness of the pork (cm)	**Pre-tuned**	**Post-tuned**
1	37.24	29.75
2	43.71	38.92
3	48.64	46.93
4	47.33	54.62
5	47.31	43.77

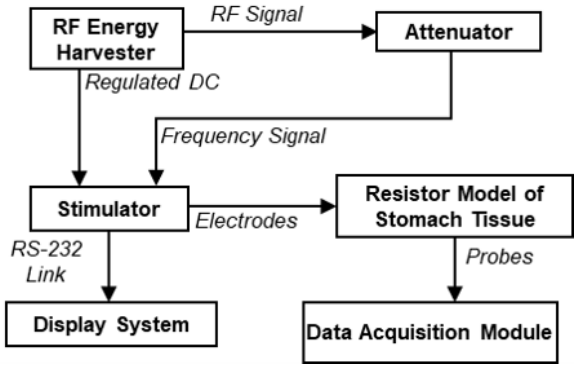

Fig. 4.22. Experimental setup for re-configurability test of the gastric stimulator.

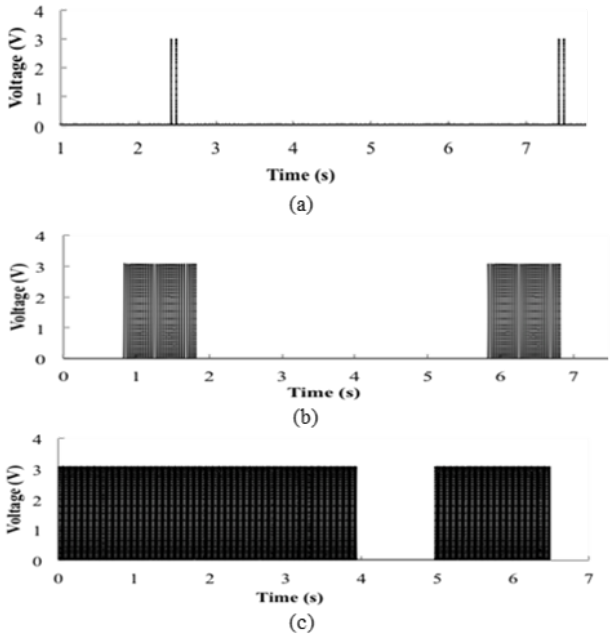

Fig. 4.23. Stimulation pulses from gastric stimulator. (a) Low setting. (b) Medium setting. (c) High setting

4.1.2 Stimulation Experiment

Figure 4.22 depicts the block diagram of the stimulator configuration for the bench top experiments where the electrodes from the stimulator were connected to a 500-Ω

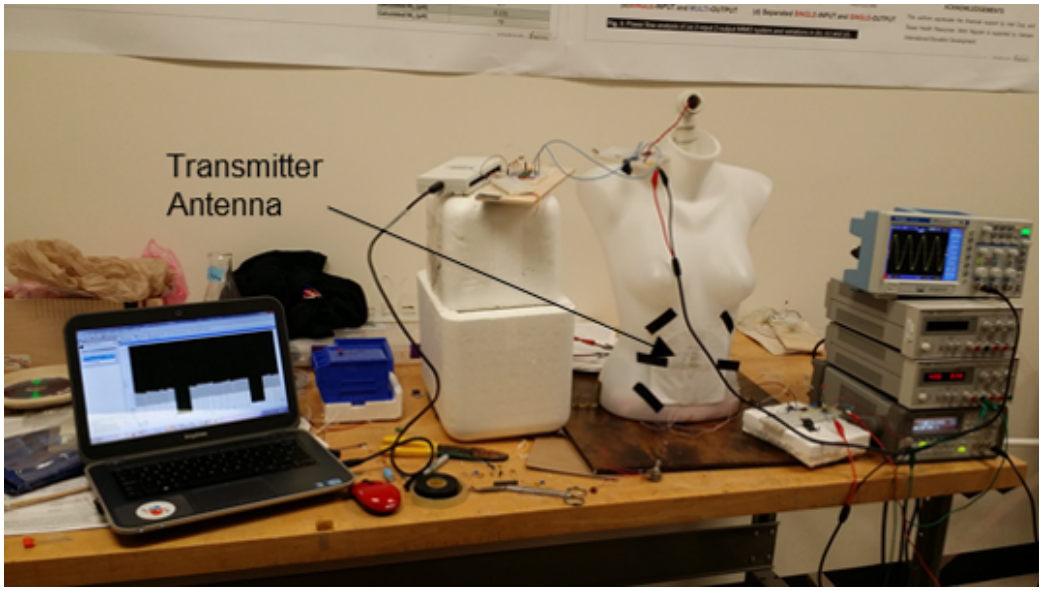

Fig. 4.24. Experimental setup of the mannequin model.

resistor which mimics the stomach muscle impedance for 1-cm apart electrodes [17]. The stimulation pulses delivered to the tissues were recorded using NI-SignalExpress and a data acquisition module (NI-USB-6211). The counted carrier frequencies were simultaneously monitored through a RS-232 interface from the stimulator to observe the reconfiguration in real time. The stimulator was reconfigured among three different settings using the aforementioned algorithm. The stimulation pulses from the gastric stimulator are shown in Fig. 4.23.

In vivo studies for a gastric stimulator was demonstrated with pig models in our earlier works [16], [17]. The live animal experiments demonstrated the feasibility, however it was difficult to obtain quantitative data with a controlled and repeatable environment due to time constrain for anesthesia, limited physical space inside stomach for wires to acquire data to verify, and varying physiological conditions in animals during experiments. Hence, an anatomical model mimicking human body environment was constructed using a mannequin shown in Fig. 4.24. The stimulator was placed inside the stomach area of the mannequin and the torso space was filled

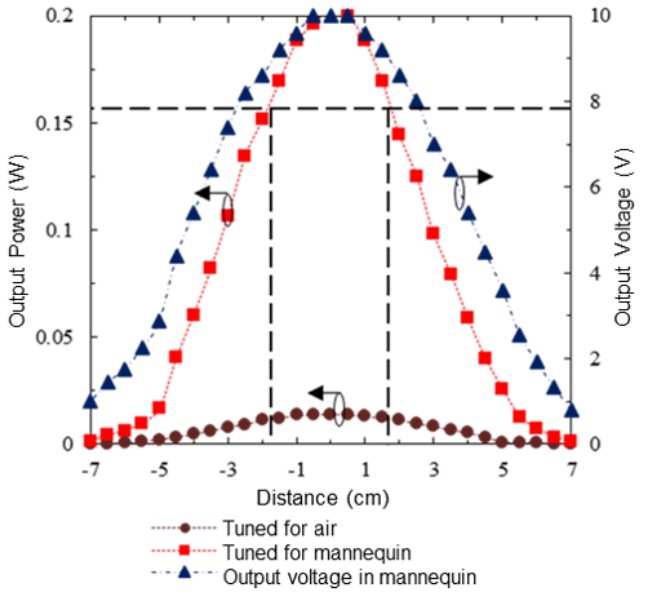

Fig. 4.25. Stimulator functionality test for misalignment in mannequin model.

with ground pork and saline mixture wrapped in plastic bags. The flexible transmitter antenna was attached outside to the abdomen area conformed to the curvature of the mannequin. Stimulator electrodes were connected through the mannequin to the data acquisition module to record the stimulation pulses. The harvested voltage waveforms from the wireless power across the module was also recorded.

Figure 4.25 shows the received power and voltage across the module as the transmitting coil was positioned with misalignment to the receiver position. Before the "implantation", the antennas were tuned in air at 4-cm separation initially. The output power became low after the "implantation" as shown in Fig. 4.25 (data labeled in circle). However, re-tuning the transmitter increased the harvested power up to the level required for operation of the gastric stimulator (data labeled in square). The receiver output power dropped as misalignment between transmitter and receiver coil increased. However, the system was able to sustain its functionality with a maximum misalignment distance of 1.5 cm in both side.

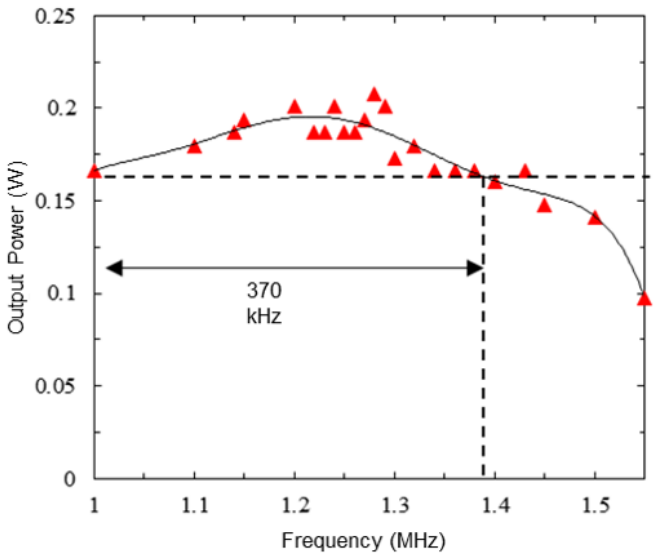

Fig. 4.26. Output power variation in the mannequin model.

4.1.3 Reconfiguration and Finding N_s, Δf_{min}

The reconfiguration of gastric stimulator was also investigated in the mannequin model by tuning the transmitter circuit over a frequency band of 1–1.55 MHz. In Fig. 4.26 each data points represents the output power after reconfiguration at the corresponding frequencies. A bandwidth (Δf_{max}) of 370 kHz was found to be available, as the output power was above 160 mW to deliver the required currents to tissues, for the remote reconfiguration method as discussed in System Design earlier.

The resolution Δf_{min} was obtained by testing the re-configurability for different sets of frequency spacing Δf and distance of separation x between transmitter and receiver. The mode change operations were triggered for three different settings. Table 4.2 summarizes the results. S_1, S_2 and S_3 represent the three different settings. The results were marked with "1" if the device could start with desired new settings during mode-change operation and with "0" in case of failure. The minimal resolution of the counter was found to be 4 kHz for a distance up to 6 cm. After the setting change, the transmitter capacitor can be re-tuned to the new frequency so the transfer

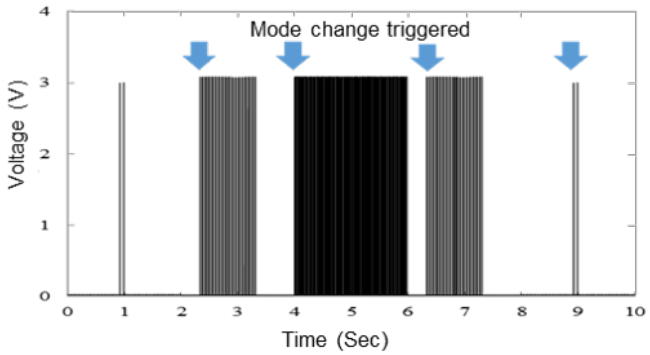

Fig. 4.27. Demonstration of remote reconfiguration of the gastrostimulator.

efficiency can be maximized. The maximum number of settings possible for the chosen receiver can be obtained by

$$N_s = \frac{\Delta f_{max}}{\Delta f_{min}} \tag{4.4}$$

Since only three settings were required for this stimulator, N_s were fixed to 3. Figure 4.27 shows the successful remote reconfiguration and the stimulation pulses were changed between three different settings using the carrier frequency modulation technique as discussed earlier.

Table 4.2.
RECONFIGURATION TESTS

Δf	**x = 4 cm**			**x = 5 cm**			**x = 6 cm**		
(kHz)	**S_1**	**S_2**	**S_3**	**S_1**	**S_2**	**S_3**	**S_1**	**S_2**	**S_3**
8	1	1	1	1	1	1	1	1	1
7	1	1	1	1	1	1	1	1	1
6	1	1	1	1	1	1	1	1	1
5	1	1	1	1	1	1	1	1	1
4	**1**	**1**	**1**	**1**	**1**	**1**	**1**	**1**	**1**
3	1	0	1	1	0	1	1	0	1
2	0	0	0	0	0	0	0	0	0

4.2 Flexible Gastrostimulator

4.2.1 Wireless Power Transfer

Several benchtop studies were performed to characterize transmitter and receiver coils used for wireless power harvesting for the gastrostimulator. The transmitter and receiver coils were tuned to resonate at 6.78 MHz by adjusting the tuning capacitances C_T and C_R. The WPT system was characterized by connecting the tuned transmitter and receiver coils to a two port vector network analyzer (Agilent N9932A) and measuring the scattering parameters.

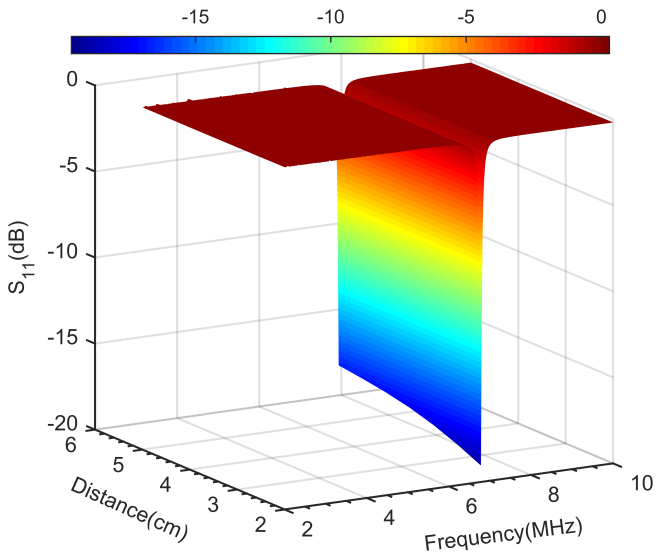

Fig. 4.28. Magnitudes of the return losses from the transmitter antenna for various antenna separation distances in air.

Effect of Distance

To analyze the effect of coil separation distance, the transmitting coil was kept stationary with the receiving coil moving at a step of 0.5 cm in a range of 2–6 cm, with the center of the both antenna aligned to each other. The reflection coefficient S_{11}

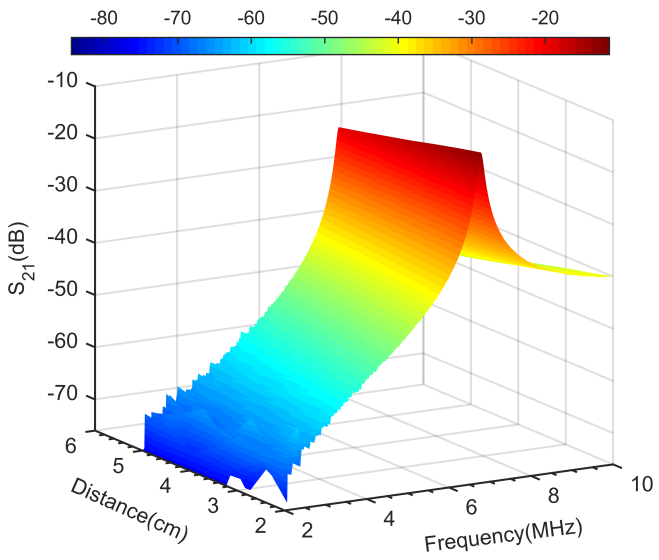

Fig. 4.29. Voltage gains of the WPT system at various distances in air.

and antenna gain S_{21} was measured over a frequency range of 2–10 MHz. Figure 4.28 shows the return loss characteristics of the transmitting coil. Since, the transmitter and receiver were tuned at 2-cm separation, the minimum S_{11} was found to be -19.04 dB at the resonant frequency for 2-cm coil separation distance. The voltage gain of the system at various distances is shown in Fig. 4.29. The maximum S_{21} at the resonant frequency was -12.64 dB for 2-cm separation and further decreased at a rate of 1.1 dB/cm for increasing the distance up to 6 cm.

Additionally, the power analysis was done at transmitting power level of 6.6 W by feeding the transmitter circuit through the class-E amplifier. A 5-V square wave with a 50% duty cycle at 6.78 MHz drove the amplifier. A 500-Ω resistor was used as the load. The power received was calculated by,

$$P_r = \frac{V_{Lrms}^2}{R_L} \tag{4.5}$$

V_{Lrms} is the root mean square (rms) voltage across the load. The wireless power transfer efficiency was obtained by,

$$\eta_{eff} = \frac{P_{out}}{P_{in}} = \frac{P_r}{V_{dd} \times I_{dd}} \tag{4.6}$$

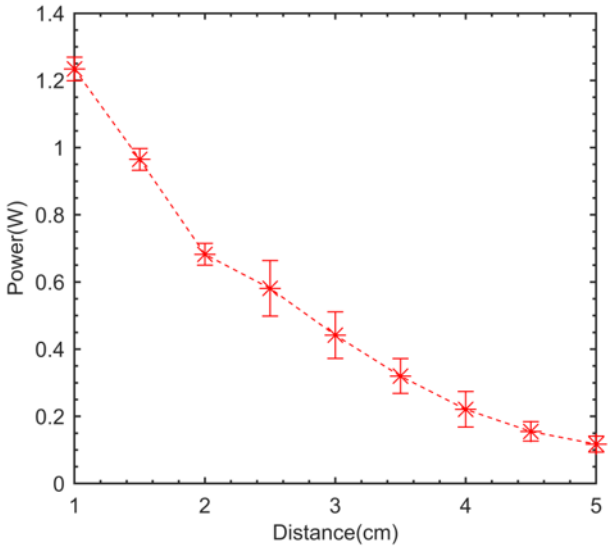

Fig. 4.30. Harvested wireless power at the flexible receiver antenna for various antenna separation distances in air.

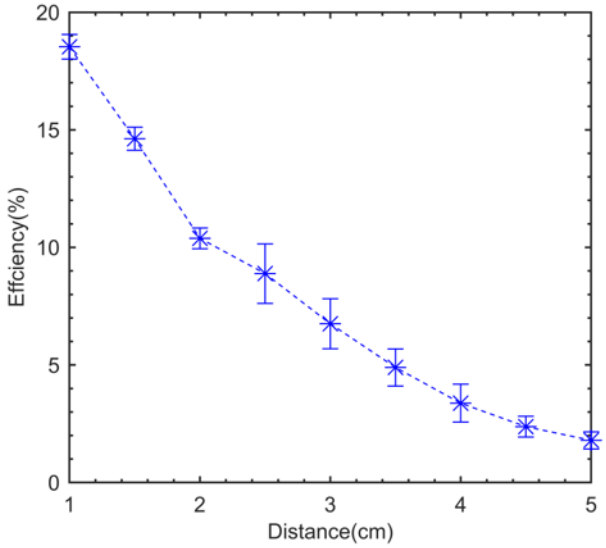

Fig. 4.31. Efficiencies of WPT using flexible receiver antenna at various antenna separation distances.

V_{dd} and I_{dd} are the DC input voltage and current, respectively, on the transmitting circuit. Figure 4.30 and 4.31 show the harvested power at receiver and WPT efficiencies of the system at various distances. The experiment was repeated three times to plot the error bars. Maximum received power was 1.23 W at the 1-cm separation with a power transfer efficiency of 18.53% and efficiencies above 3% were maintained for distances up to 4 cm. The minimum harvested power at the 5-cm distance was 117 mW which was adequate for the gastrostimulator device to be functional.

Effect of Misalignment

In practical scenarios the implant will not be perfectly aligned to the transmitter antenna owing to various factors like stomach movements, placement of the device during surgery and the fact that the patients do not know the exact location before they put on the belt every morning. It is important to study the power transfer effect from misalignment. The tuned transmitter antenna was kept fixed and tuned receiver antenna was moved precisely with a step of 0.5 cm in the cross section plane facing the transmitter at various distances using a programmed mechanical robot as shown in Fig. 4.32. The robot was operated by two stepper motors for movement of the receiving antenna in X and Y directions. The robot arm was controlled by a LabVIEW program designed for actuation and subsequent data accusation using the VNA. Shown in Fig. 4.33, 50% of the maximum antenna gain, which was the gain with perfect center-to-center alignment, was maintained within a 3 cm $\times$ 3 cm area on the cross section plane for all the distances.

Effect of Bending

Since, the flexible gastric stimulator will be placed inside the sub-mucosal layer of the stomach, it is going to bend with peristalsis movement of the stomach. It was very crucial to investigate WPT performance degradation at resonant frequency due to flexing of the receiver antenna. The curvature radius of the stomach varies in the

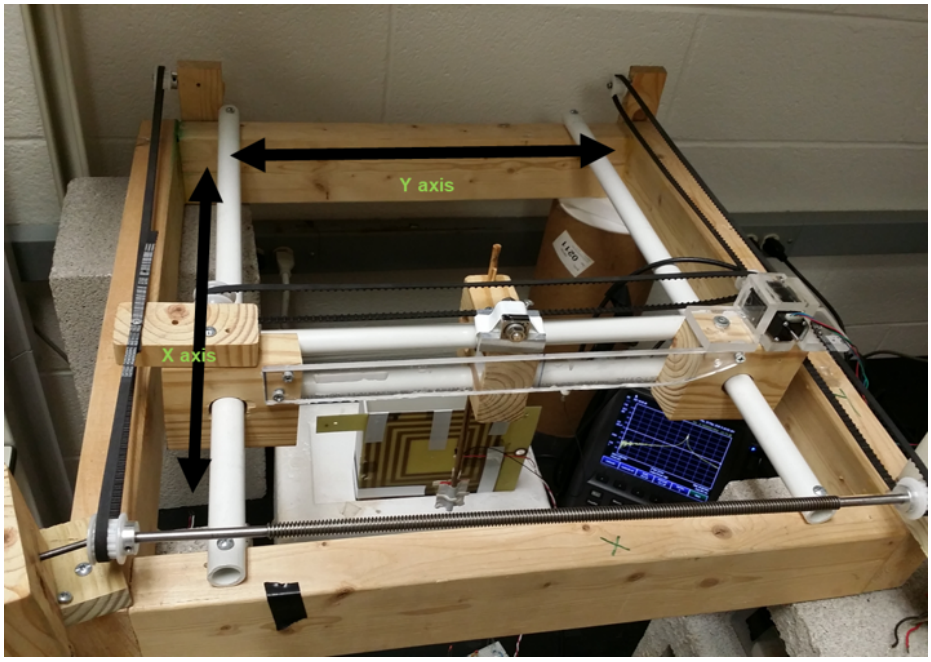

Fig. 4.32. Automated robot for field distribution mapping of WPT antennas.

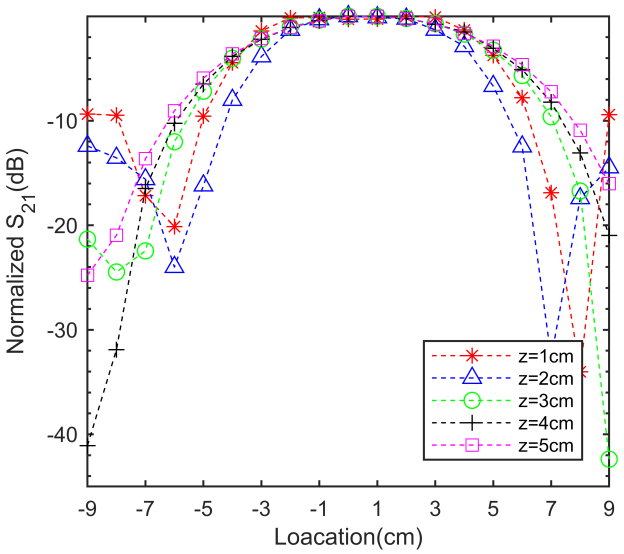

Fig. 4.33. Effect of antenna misalignment on gain of the WPT system at various antenna separation distances.

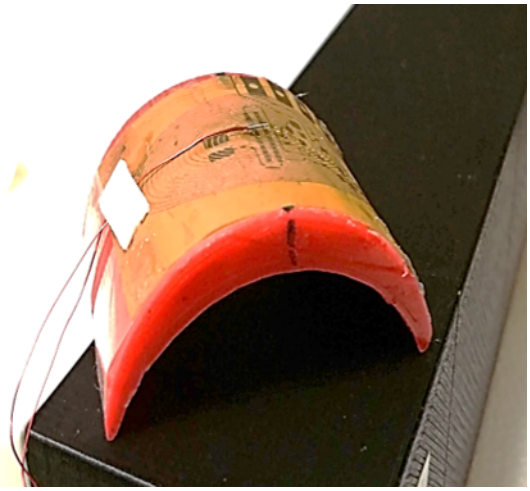

Fig. 4.34. The flexible gastrostimulator antenna attached to the 3-D printed structure with 2-cm curvature radius.

range of 2–4 cm during the peristalsis movement [39]. 3-D structures with precise curvature radiuses 2, 4, 6 and 8 cm were printed using polylactic acid (PLA) and a 3-D printer. The receiver antenna was attached to the curved printed structure as shown in Fig. 4.34. The antennas were tuned and placed at a 4-cm separation distance with receiver antenna curving away from the transmitter antenna.

Figure 4.35 shows the gain measurements with various bending curvature radius over frequency range of 2–10 MHz. The gain, at worst case scenario i.e. when the receiver was curved at 2-cm curvature radius, was -22.81 dB which was 8.4% less compared to the 8-cm curvature radius.

Effect of Dielectric Layers

The presence of tissues between the coils was expected to have an effect on the power transfer due to dielectric properties changing the mutual inductance and parasitic capacitance. Apart from resonant frequency shifts and conductive losses, it also results in input impedance change of the transmitter. Like rigid gastrostimulator 0.9% saline and ground beef was used to mimic human body tissues. They were

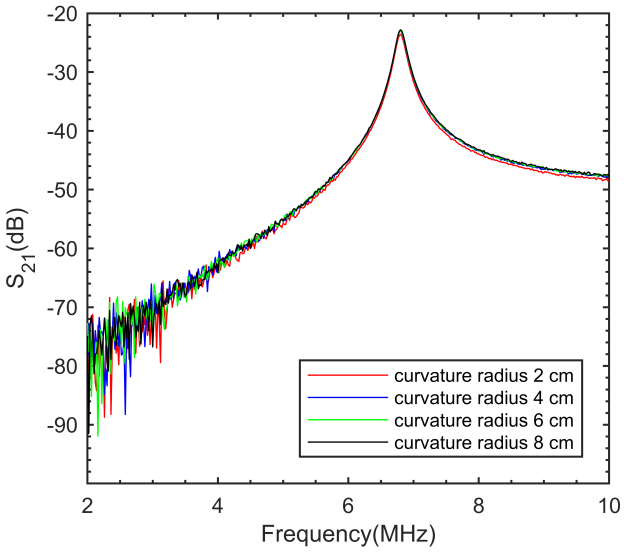

Fig. 4.35. Effect of the receiver antenna bending on gain of the WPT system at 4-cm antenna separation distances.

Fig. 4.36. Experimental setup of the dielectric layer experiment. The left photo shows the position of the receiver antenna with tuning capacitor on the 3-D printed box filled with ground beef and the right photo shows the transmitter antenna attached to the other side of the box.

both studied for effects in loss and resonance frequency shifts. The experiments were conducted by placing these dielectric materials between coils. Shown in Fig. 4.36, the ground beef, moist with phosphate buffered saline, and saline were kept in 15 cm

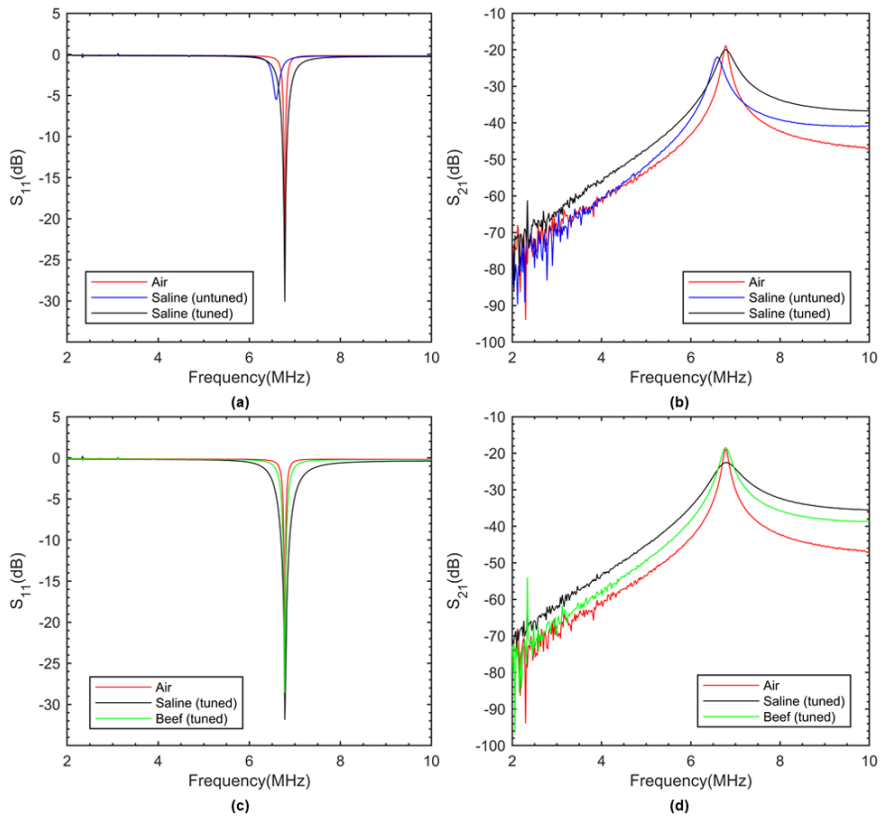

Fig. 4.37. (a) Comparison of magnitudes of return losses of WPT system for dielectric medium air, saline (un-tuned) and saline (tuned by impedance matching), (b) Change in voltage gain of the WPT system due to air, saline (un-tuned) and saline (tuned), (c) Comparison of magnitudes of return losses of WPT system for dielectric medium air, saline (tuned) and ground beef (tuned), (d) Change in voltage gain of the WPT system due to air, saline (tuned) and ground beef (tuned).

$\times$ 15 cm $\times$ 4 cm thin plastic box to investigate the dielectric effects. Initially, the transmitter and receiver were attached to the outer side walls of the empty box at a spacing of 4 cm in air and matched to 50-Ω source impedance at resonant frequency by impedance matching technique. Then the 0.9% saline solution was added in the box and reflection coefficient and antenna gains were measured and compared in Fig. 4.37(a) and (b). The S_{11} was -26.24 dB at resonant frequency 6.78 MHz for air and with the saline the resonant frequency shifted to 6.6 MHz with 20.77 dB increase

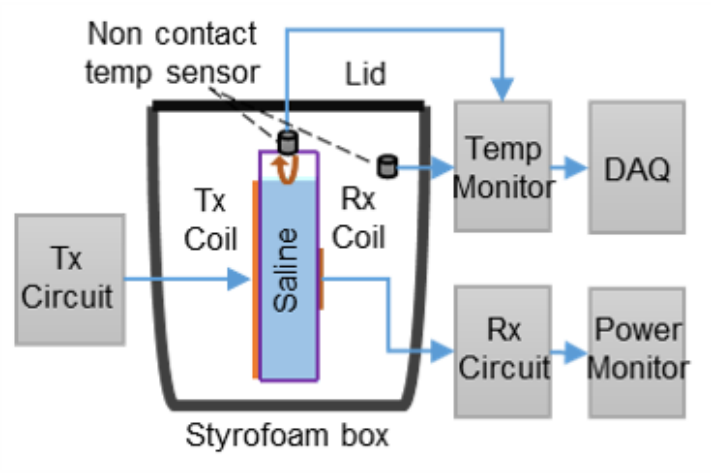

Fig. 4.38. Experimental setup of temperature study for WPT through saline.

in reflection signal due to impedance mismatch caused by saline. However, when the impedance matching circuit at transmitter circuit was re-tuned for saline the S_{11} improved to -30.05 dB at 6.78 MHz. Figure 4.37(b) compares the antenna gains in air, saline with and without tuning. The gain peak in air was -18.37 dB at resonant frequency and dropped by 3.13 dB and shifted to 6.6 MHz for saline. However, with impedance matching a -19.99 dB of maximum gain could be achieved at resonant frequency. Figure 4.37(c) and (d) shows comparison of antenna performance in air, saline and beef with impedance matching. The S_{11} were observed to be very similar for all the cases. The S_{21} were -18.37, -22.57 and -18.45 dB for air, saline and beef respectively. The gain in saline was minimum due to resistive loss in presence Na^{+} and Cl^{-} ions in saline solution. The loss in beef was -0.08 dB compared to the air which confirms minimal power absorption in animal tissue at 6.78 MHz and further enhances safety of the device.

Temperature Study

Even though the gastric stimulation device needs to be turned on during food consumption and few hours after consumption. An experiment was designed to in-

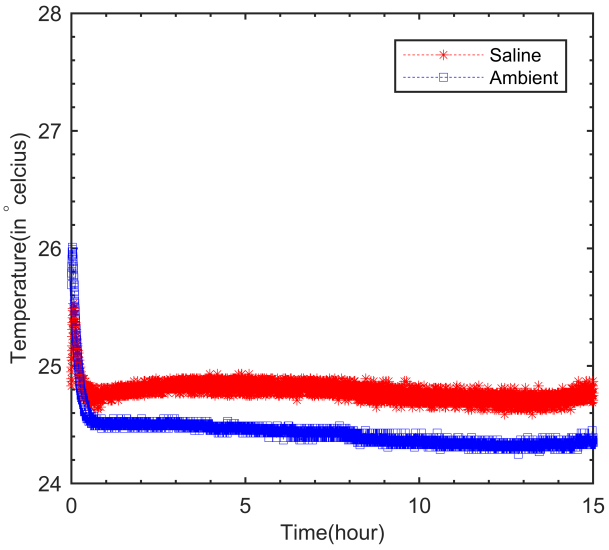

Fig. 4.39. The effect of long duration WPT on dielectric temperature increment in open environment.

vestigate effect of tissue heating due to prolonged WPT. As it was found in previous section saline could be considered the worst case scenario in terms of power absorption, the WPT through saline was investigated for 15 hours at room temperature (24.45^o C). Figure 4.38 shows the experimental setup. Like previous experiment the transmitter and receiver coils were placed on the side outer walls of 15 cm $\times$ 15 cm $\times$ 4 cm thin plastic box which was filled with saline. One of the tow non-contact infrared temperature sensor (MLX90614, Melexis) was placed through a hole on the cover of the plastic box to record the temperature of the saline and other sensor was used to record the ambient temperature. The entire setup was placed in side a 38 cm $\times$ 30 cm $\times$ 20 cm box made with 4-cm thick styrofoam. The WPT transmitter and receiver circuits were tuned and connected through the sealed holes in the box. An Arduino board was used to monitor and record the saline and ambient temperature. The input power level was fixed to 3.9 W which is the minimum amount of input power required to harvest enough energy at receiver side in this setup so that, the device can provide required stimulation current.

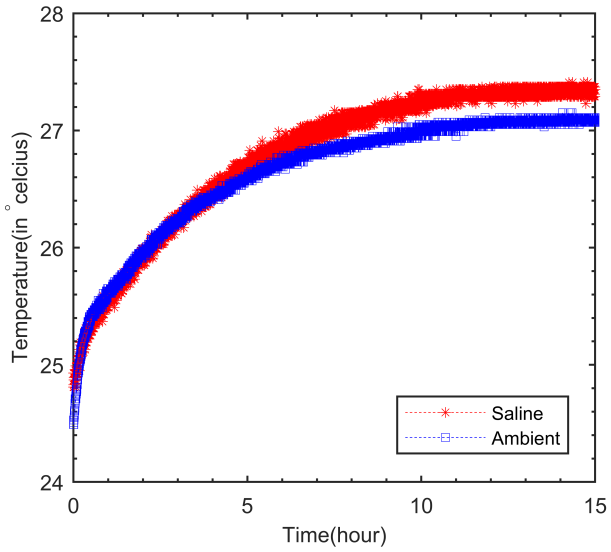

Fig. 4.40. The effect of long duration WPT on dielectric temperature increment in closed environment with lid of the styrofoam box put in place.

Figure 4.39 shows the temperature readings when the lid of the styrofoam box was open. The temperature of the saline stabilized at 24.81^o C and was increased by 1.45% compared to the ambient temperature. Similarly, Fig. 4.40 shows the temperature results when the lid of the styrofoam box was closed and the system was thermally insulated from environment. Ambinet temperature and saline temperature both increased and stabilized at 27.07 and 27.35 ^{o} C respectively. The 3.4^oC increase in temperature could be due to energy dissipation from the transmitter due to joule heating. These experiments further ensures the power absorption in the tissue during WPT at 6.78 MHz was minimal.

5. ANIMAL EXPERIMENTS

5.1 Rat Muscle Stimulation Experiments

The wireless powered flexible gastrostimulator (FlexStim) was tested for muscle stimulation in rat model. A male Sprague-Dawley rat (380 gm) was used for the animal experiment. All surgical procedures were approved by the University of Texas at Arlington Institutional Animal Care and Use Committee.

Figure 5.1 and 5.2(a) show the experimental setup and the block diagram of animal experiment. The WPT transmitter coil was attached to a 6-cm thick wooden block to eliminate the effect of metal interference in WPT and the block was placed on the surgical table. The anesthetized rat was placed above transmitter coil separated by transparency sheet. The transmitter coil was connected to the WPT transmitting circuit. Power transfer efficiencies were verified in air with a dummy receiver antenna. Once the WPT system was tuned and ready for the animal testing the rat was anesthetized using isoflurane. The back portion of the rat was trimmed to remove body hair. A 1:1 mixture of isoflurane and oxygen was used for stabilizing the rat and it was moved to the surgery table once the heart rate was stabilized at 295 beats per minute. The the stimulator was attached on the back of the rat conformal to the body shape and perfectly aligned to the transmitter coil with 5-cm of antenna separation distances. The transmitter and receiver circuits were re-tuned to compensate the dielectric frequency shift and efficiency-drop caused by the animal tissue. As shown in Fig. 5.2(c) an incision was made in the rat skin to expose the back muscle (splenius) and two electrodes are inserted 5 mm deep into the muscle at a separation distance of 1 cm. These electrodes were also connected to National Instrument DAQ module (NI-DAQ-6211) for stimulation pulse recording. Another set of electrodes (81MS2021SPCE MS303-1-B-SPC-ELECT SS 2C TW .010) were

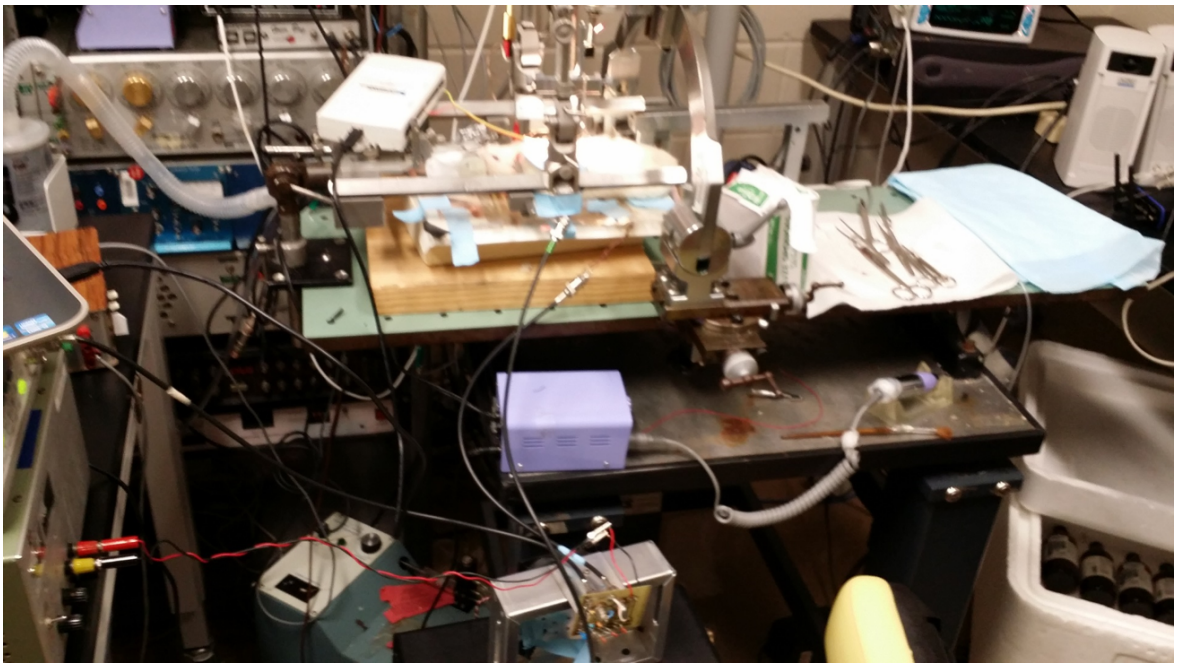

Fig. 5.1. Photo of the surgery table with wireless powered flexible gastric stimulator during muscle stimulation experiment.

inserted in to the muscle 2-cm apart from the stimulation electrodes to record the electromyogram signal from the muscle using a wireless recording module (MC Rack Multichannel Systems) and recorded signals were analyzed by MC Rack Data acquisition software at the base station. The WPT efficiencies and harvested power at resonant frequency was monitored.

The system could harvest more than 160 mW power and the stimulator provided stimulation pulsed as desired. Figure 5.2(b) shows the stimulation pulses recorded during muscle stimulation. The maximum pulse voltage was 1.3 V with 5.2 mA stimulation current injected into the muscle. The periodic muscle contraction was observed recorded in video format. The muscle stimulation were also observed in EMG recording and shown in 5.3.

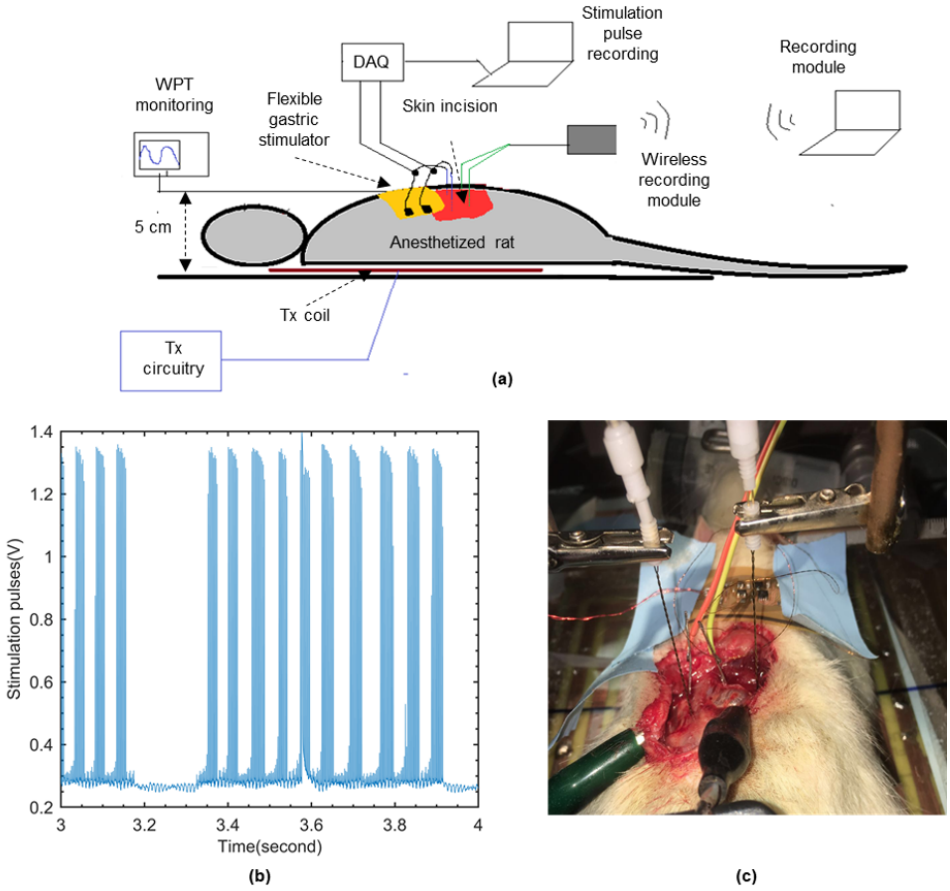

Fig. 5.2. (a) The block diagram of the animal experiment for muscle stimulation using flexible gastric stimulator. (b) Recorded stimulation pulses delivered to the muscle. (c) Photo of placement of the electrodes and the stimulator.

5.2 Validation of Submucosal Implant in Porcine Model

In this section, two different methods were investigated for the feasibility of the gastrostimulator placement in the submucosal pocket. Animal tests were performed on the porcine model, which is commonly used in gastric electrical activity and stimulation studies [40].

The animal was prepared by general anesthesia induced using zoletil and isoflurane, with continuous monitoring of vital physiological parameters and temperature.

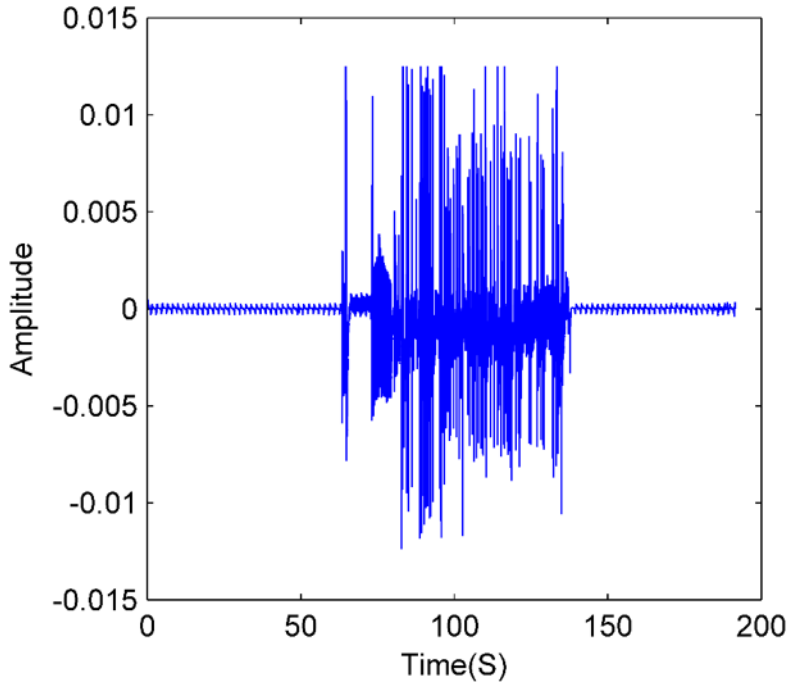

Fig. 5.3. EMG recording of the muscle during muscle stimulation using wireless powered flexible gastrostimulator.

As shown in Fig.5.4 the midline laparotomy was performed to expose the gastric serosa, followed by a vertical gastrotomy. A submucosal flap was dissected to generate a 3 cm $\times$ 1 cm pocket space deep to the circular muscle layer, simulating endoscopic mucosal dissection. Several flexible dummy gastrostimulators were fabricated by encapsulating copper coated polyimide substrate with biocompatible PDMS. The flexible dummy gastrostimulator was inserted into this pocket, with contact points embedded adjacent to the muscular layer. The flap was opposed and the mucosa secured using three Resolution (TM) endoclips, and the gastrotomy was closed using a continuous 3–0 pds suture. In three consecutive implant tests, the flexible dummy gastrostimulator could be inserted with minimal tissue disruption, secure attachment without gastric perforation or hematoma, and with a minimal profile of protrusion into the gastric lumen.

It was found that the submucosal pocket is an appropriate potential option for the implant. Figure 5.5 and 5.6 show the device was placed deep in the tissue, well protected, and making firm contact with the target muscle layer. Additionally, the absence of acid, enzymes and mucous in this place makes it more attractive for protection of implant electrodes.

The only technical challenge is to access submucosal pocket. Endoscopically implanting the device into this place would require experienced and advanced endoscopic skills, and well equipped technical unit as the challenges arrives from achieving clear visualization, endoscopic dissection, handling bleeding and in achieving secure closure of the space.

On the other hand surgically, access to the pocket is a great deal easier since. Via open surgery, it would be easy (as per this trial), as haemostasis (control of bleeding), dissection and closure by suturing is straightforward. Laparoscopically, (via minimal access keyhole surgery) it would be more challenging, but still likely very much easier and more controlled (ie. safer) than the endoscopic approach. And certainly much quicker.

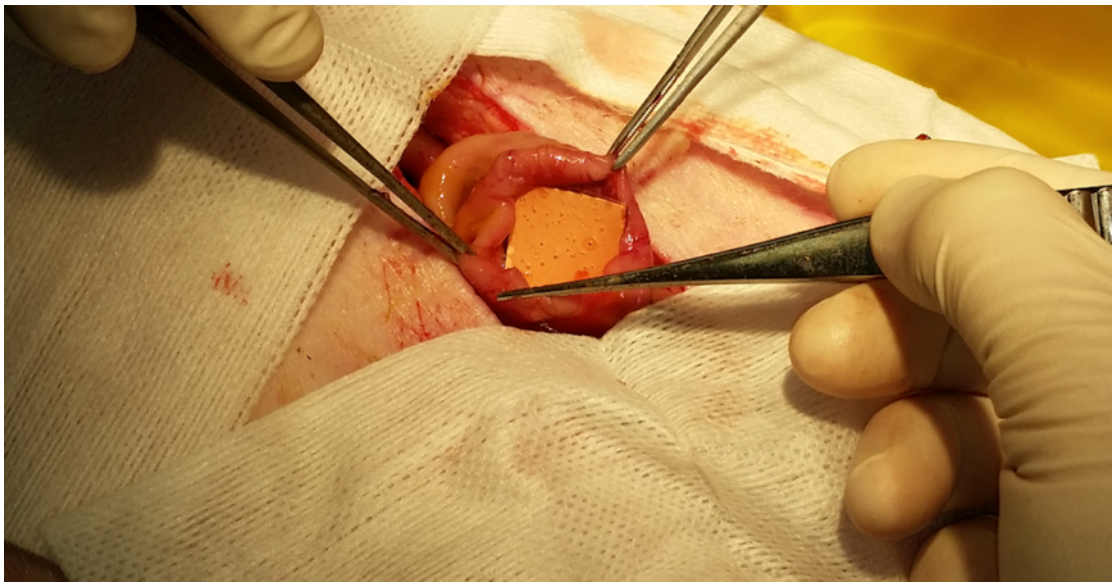

Fig. 5.4. Incision and gastric access. The photo shows the inside of the stomach with a 2 cm × 2 cm square dummy device sitting in the submucosal pocket.

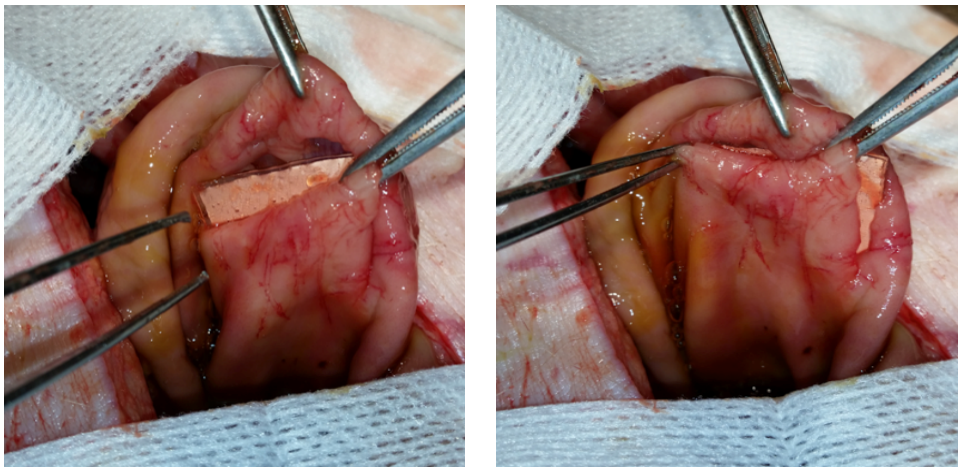

(a) (b)

Fig. 5.5. (a) Here a rectangular device (2 × 1.5 cm) was inserted in a submucosal pocket and (b) the flap opposed, from here it can be readily sutured to completely conceal the device with good tissue apposition.

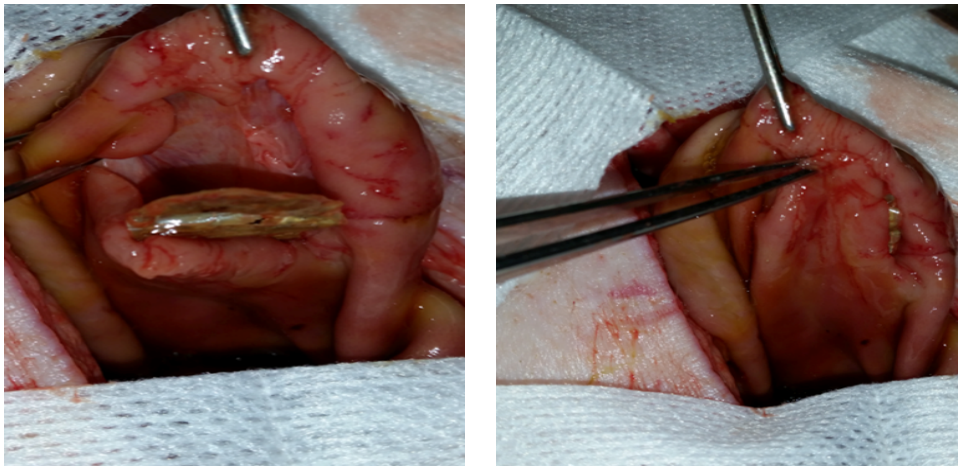

(a) (b)

Fig. 5.6. (a) The smooth deep layer (circ muscle layer) of the subcutaneous pocket flap, being a comfortable secure space for this device to sit (Dummy Stimulator). (b) This photo shows again how the flap can be laid back over the device to achieve a good fit – from here, it can be readily sutured to completely/snugly secure the device within the tissue space.

6. CONCLUSION AND FUTURE WORK

6.1 Conclusion

In this work, two miniature implantable gastric stimulation devices were conceptualized and fabricated. Both the devices were designed to operate with out a battery and powered using a wireless power transfer system.

The first prototype device was a rigid stimulator with a device volume 95% smaller than the commercially available stimulator used for GES treatment. The implant antenna designs of the rigid stimulator were optimized for efficient energy harvesting performance. The WPT system was characterized by conducting various benchtop studies. The system was tested with different thicknesses of pork and 0.9% saline between the transmitter and receiver antennas to determine power losses and effects on resonance in the system. Inductive coupling was demonstrated not only for providing power but also for remote communication of the device. A new re-configurability method was proposed, tested and the available bandwidth for the operation was determined. A 370-kHz bandwidth was measured, sufficient for remote re-configurability of the stimulator. A $\pm$1.8-cm misalignment from the centers of the coils will still provide enough power to operate. These measured results show that the device can work well in human with a tissue thickness up to 4 cm. A mannequin constructed to mimic body conditions was used to validate the benchtop experiment results.

In the second part of the work, more advanced a flexible gastrostimulator was fabricated using standard photolithography technique. The substrate and metal layers were optimized for bending and rolling. The monolithic implant antenna was optimized for 6.78 MHz frequency. The WPT system of the flexible gastrostimulator was characterized for antenna separation distance and misalignment. The antenna voltage gain at resonant frequency dropped by 1.1 dB per cm. At 5-cm antenna sep-

aration, a minimum of 117 mW power was harvested at the implant side. The effect of antenna bending due to stomach movement was also investigated and it was found that bending in worst case scenario only contributes 8.4% reduction in energy harvesting performance. The effect of animal tissue during wireless power transfer was also characterized. Unlike rigid stimulator, with impedance matching technique, insertion losses caused by the change in input impedance for dielectric layers were avoided for the flexible gastric stimulator. A -0.08 dB of the tissue attenuation loss was measured for 4-cm of a ground beef layer. Safety issues with tissue heating during prolonged WPT were further addressed by a controlled temperature study experiment. Finally, the wireless powered flexible gastric stimulator was demonstrated by stimulating the back muscle of a rat. Additionally, feasibility of submucosal implant was also investigated in porcine model.

6.2 Future Work

With the current design, the efficacy of the treatment would be analyzed based on the feedback from the patient. Since the gastrostimulator will be placed in submucosal place, it will also flex during the peristalsis of the stomach. In future, the stomach motility tracking could be investigated by incorporating a strain sensor to the flexible gastric stimulator. The strain information can be encoded and communicated back to the transmitter by modulating the load of the implant which will generate variation in the transmitter current. The encoded strain information could be extracted by using envelope detector at transmitter circuit.

The electrode design of the gastrostimulator can also be improved. By measuring the impedance between the electrodes, the postoperative bacterial infection at implant site could be identified from outside. A micro-fluidic channel could be designed within flexible gastrostimulator and filled with an antibiotic drug so that, if bacterial infections are detected, antibiotic drugs can be delivered on the implant side at certain intervals. Figure 6.1 shows the next generation flexible gastric stimulator, apart

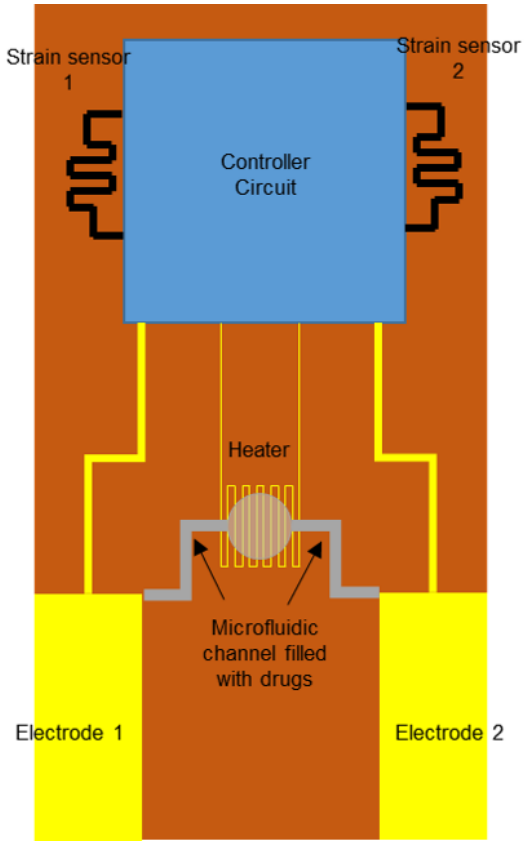

Fig. 6.1. Advance design of flexible gastric stimulator with strain sensor for stomach motility tracking and self healing drug delivery technique.

from the strain sensors for stomach motility tracking it also has a drug delivery unit to keep the electrodes infection free. The heater under micro-fluidic chamber can be turned on, to deliver antibiotic drugs to the electrodes.

REFERENCES

REFERENCES

[1] J. Tack and N. J. Talley, "Functional dyspepsia–symptoms, definitions and validity of the rome iii criteria." *Nat Rev Gastroenterol Hepatol*, vol. 10, no. 3, pp. 134–141, mar 2013. [Online]. Available: http://dx.doi.org/10.1038/nrgastro.2013.14

[2] V. Wadhwa, D. Mehta, Y. Jobanputra, R. Lopez, P. N. Thota, and M. R. Sanaka, "Healthcare utilization and costs associated with gastroparesis." *World J Gastroenterol*, vol. 23, no. 24, pp. 4428–4436, jun 2017. [Online]. Available: http://dx.doi.org/10.3748/wjg.v23.i24.4428

[3] Y. R. Wang, R. S. Fisher, and H. P. Parkman, "Gastroparesis-related hospitalizations in the united states: trends, characteristics, and outcomes, 1995-2004." *Am J Gastroenterol*, vol. 103, no. 2, pp. 313–322, feb 2008. [Online]. Available: http://dx.doi.org/10.1111/j.1572-0241.2007.01658.x

[4] S. Deb, "Miniature wireless gastrostimulator," Ph.D. dissertation, The University of Texas at Arlington, 2011.

[5] T. Abell, R. McCallum, M. Hocking, K. Koch, H. Abrahamsson, I. Leblanc, G. Lindberg, J. Konturek, T. Nowak, E. M. M. Quigley, G. Tougas, and W. Starkebaum, "Gastric electrical stimulation for medically refractory gastroparesis." *Gastroenterology*, vol. 125, no. 2, pp. 421–428, aug 2003. [Online]. Available: http://linkinghub.elsevier.com/retrieve/pii/S0016508503008783

[6] R. W. McCallum, S. C. Polepalle, and B. Schirmer, "Completion gastrectomy for refractory gastroparesis following surgery for peptic ulcer disease. long-term follow-up with subjective and objective parameters." *Dig Dis Sci*, vol. 36, no. 11, pp. 1556–1561, nov 1991. [Online]. Available: https://www.ncbi.nlm.nih.gov/pubmed/1935493

[7] I. Soykan, B. Sivri, I. Sarosiek, B. Kiernan, and R. W. McCallum, "Demography, clinical characteristics, psychological and abuse profiles, treatment, and long-term follow-up of patients with gastroparesis." *Dig Dis Sci*, vol. 43, no. 11, pp. 2398–2404, nov 1998. [Online]. Available: https://www.ncbi.nlm.nih.gov/pubmed/9824125

[8] T. L. Abell, E. Van Cutsem, H. Abrahamsson, J. D. Huizinga, J. W. Konturek, J. P. Galmiche, G. VoelIer, L. Filez, B. Everts, W. E. Waterfall, W. Domschke, S. Bruley des Varannes, B. O. Familoni, I. M. Bourgeois, J. Janssens, and G. Tougas, "Gastric electrical stimulation in intractable symptomatic gastroparesis." *Digestion*, vol. 66, no. 4, pp. 204–212, 2002. [Online]. Available: http://dx.doi.org/68359

[9] B. E. Bellahsene, C. D. Lind, B. D. Schirmer, O. L. Updike, and R. W. McCallum, "Acceleration of gastric emptying with electrical stimulation in a canine model of gastroparesis," *American Journal of Physiology-Gastrointestinal*

and Liver Physiology, vol. 262, no. 5, pp. G826–G834, may 1992. [Online]. Available: http://www.physiology.org/doi/10.1152/ajpgi.1992.262.5.G826

[10] R. W. McCallum, J. De Z. Chen, Z. Lin, B. D. Schirmer, R. D. Williams, and R. A. Ross, "Gastric pacing improves emptying and symptoms in patients with gastroparesis," *Gastroenterology*, vol. 114, no. 3, pp. 456–461, mar 1998. [Online]. Available: http://linkinghub.elsevier.com/retrieve/pii/S0016508598705281

[11] B. O. Familoni, T. L. Abell, D. Nemoto, G. Voeller, and B. Johnson, "Efficacy of electrical stimulation at frequencies higher than basal rate in canine stomach," *Digestive Diseases and Sciences*. [Online]. Available: https://link.springer.com/article/10.1023/A:1018804128695

[12] B. O. Familoni, T. L. Abell, G. Voeller, A. Salem, and O. Gaber, "Electrical stimulation at a frequency higher than basal rate in human stomach." *Dig Dis Sci*, vol. 42, no. 5, pp. 885–891, may 1997. [Online]. Available: https://www.ncbi.nlm.nih.gov/pubmed/9149038

[13] J. Forster, I. Sarosiek, R. Delcore, Z. Lin, G. S. Raju, and R. W. McCallum, "Gastric pacing is a new surgical treatment for gastroparesis." *Am J Surg*, vol. 182, no. 6, pp. 676–681, dec 2001. [Online]. Available: https://www.ncbi.nlm.nih.gov/pubmed/11839337

[14] M. P. Jones, C. C. Ebert, and K. Murayama, "Enterra for gastroparesis," *Am J Gastroenterol*, vol. 98, no. 11, pp. 2578–2578, nov 2003. [Online]. Available: http://www.nature.com/doifinder/10.1111/j.1572-0241.2003.08681.x

[15] S. Dubey and J.-C. Chiao, "Power transfer for a flexible gastric stimulator," in *2016 IEEE Topical Conference on Biomedical Wireless Technologies, Networks, and Sensing Systems (BioWireleSS)*. IEEE, jan 2016, pp. 15–17. [Online]. Available: http://ieeexplore.ieee.org/document/7445549/

[16] S. Deb, S.-J. Tang, T. L. Abell, S. Rao, W.-D. Huang, S. D. F. To, C. Lahr, and J.-C. Chiao, "An endoscopic wireless gastrostimulator (with video)." *Gastrointest Endosc*, vol. 75, no. 2, pp. 411–5, 415.e1, feb 2012. [Online]. Available: http://dx.doi.org/10.1016/j.gie.2011.09.052

[17] S. Rao, S. Dubey, S. Deb, Z. Hughes, Y.-S. Seo, M. Q. Nguyen, S.-J. Tang, T. Abell, C. Lahr, and J.-C. Chiao, "Wireless gastric stimulators," in *Texas Symposium on Wireless and Microwave Circuits and Systems*. IEEE, apr 2014, pp. 1–4. [Online]. Available: http://ieeexplore.ieee.org/lpdocs/epic03/wrapper.htm?arnumber=7015875

[18] M. Ghovanloo and S. Atluri, "A wide-band power-efficient inductive wireless link for implantable microelectronic devices using multiple carriers," *IEEE Trans. Circuits Syst. I*, vol. 54, no. 10, pp. 2211–2221, oct 2007. [Online]. Available: http://ieeexplore.ieee.org/lpdocs/epic03/wrapper.htm?arnumber=4346666

[19] Y.-X. Guo, D. Zhu, and R. Jegadeesan, "Inductive wireless power transmission for implantable devices," in *2011 International Workshop on Antenna Technology (iWAT)*. IEEE, mar 2011, pp. 445–448. [Online]. Available: http://ieeexplore.ieee.org/lpdocs/epic03/wrapper.htm?arnumber=5752354

[20] F. Zhang, X. Liu, S. A. Hackworth, R. J. Sclabassi, and M. Sun, "In vitro and in vivo studies on wireless powering of medical sensors and implantable devices," in *2009 IEEE/NIH Life Science Systems and Applications Workshop*. IEEE, apr 2009, pp. 84–87. [Online]. Available: http://ieeexplore.ieee.org/lpdocs/epic03/wrapper.htm?arnumber=4906715

[21] X. Li, C.-Y. Tsui, and W.-H. Ki, "A 13.56 mhz wireless power transfer system with reconfigurable resonant regulating rectifier and wireless power control for implantable medical devices," *IEEE J. Solid-State Circuits*, vol. 50, no. 4, pp. 978–989, apr 2015. [Online]. Available: http://ieeexplore.ieee.org/document/7035125/

[22] P. Si, A. P. Hu, S. Malpas, and D. Budgett, "A frequency control method for regulating wireless power to implantable devices." *IEEE Trans Biomed Circuits Syst*, vol. 2, no. 1, pp. 22–29, mar 2008. [Online]. Available: http://dx.doi.org/10.1109/TBCAS.2008.918284

[23] P. Li and R. Bashirullah, "A wireless power interface for rechargeable battery operated medical implants," *IEEE Trans. Circuits Syst. II*, vol. 54, no. 10, pp. 912–916, oct 2007. [Online]. Available: http://ieeexplore.ieee.org/lpdocs/epic03/wrapper.htm?arnumber=4349228

[24] S. Kim, J. S. Ho, L. Y. Chen, and A. S. Y. Poon, "Wireless power transfer to a cardiac implant," *Appl Phys Lett*, vol. 101, no. 7, p. 073701, aug 2012. [Online]. Available: http://scitation.aip.org/content/aip/journal/apl/101/7/10.1063/1.4745600

[25] "Ieee standard for safety levels with respect to human exposure to radio frequency electromagnetic fields, 3 khz to 300 ghz," IEEE, Standard.

[26] G. Kendir, W. Liu, G. Wang, M. Sivaprakasam, R. Bashirullah, M. Humayun, and J. Weiland, "An optimal design methodology for inductive power link with class-e amplifier," *IEEE Trans. Circuits Syst. I*, vol. 52, no. 5, pp. 857–866, may 2005. [Online]. Available: http://ieeexplore.ieee.org/lpdocs/epic03/wrapper.htm?arnumber=1427894

[27] M. Q. Nguyen, Z. Hughes, P. Woods, Y.-S. Seo, S. Rao, and J.-C. Chiao, "Field distribution models of spiral coil for misalignment analysis in wireless power transfer systems," *IEEE Trans Microw Theory Tech*, vol. 62, no. 4, pp. 920–930, apr 2014. [Online]. Available: http://ieeexplore.ieee.org/lpdocs/epic03/wrapper.htm?arnumber=6729099

[28] H. C. Gonzalez and V. Velanovich, "Enterra therapy: gastric neurostimulator for gastroparesis." *Expert Rev Med Devices*, vol. 7, no. 3, pp. 319–332, may 2010. [Online]. Available: http://dx.doi.org/10.1586/erd.10.4

[29] *Low-Power Sub-1 GHz RF Transceiver*, Texas Instrument, rev. 1.

[30] H. Park, J.-S. Park, Y. Pu, S.-O. Lim, Y.-K. Moon, S.-H. Kim, and K.-Y. Lee, "A design of high efficiency class-e power amplifier for wireless power transfer system," in *2011 IEEE MTT-S International Microwave Workshop Series on Intelligent Radio for Future Personal Terminals*. IEEE, aug 2011, pp. 1–2. [Online]. Available: http://ieeexplore.ieee.org/document/6027207/

[31] "www.dupont.com/content/dam/dupont/products-and-services/electronic-and-electrical-materials/flexible-rigid-flex-circuit-materials/documents/pyraluxapclad_datasheet.pdf."

[32] P. E. Donaldson, "The encapsulation of microelectronic devices for long-term surgical implantation." *IEEE Trans Biomed Eng*, vol. 23, no. 4, pp. 281–285, jul 1976. [Online]. Available: https://www.ncbi.nlm.nih.gov/pubmed/1278923

[33] S. H. Kim, J.-H. Moon, J. H. Kim, S. M. Jeong, and S.-H. Lee, "Flexible, stretchable and implantable pdms encapsulated cable for implantable medical device," *Biomed Eng Lett*, vol. 1, no. 3, pp. 199–203, aug 2011. [Online]. Available: http://link.springer.com/10.1007/s13534-011-0033-8

[34] C. J. Lahr, J. Griffith, C. Subramony, L. Halley, K. Adams, E. R. Paine, R. Schmieg, S. Islam, J. Salameh, D. Spree, T. Kothari, A. Kedar, Y. Nikitina, and T. Abell, "Gastric electrical stimulation for abdominal pain in patients with symptoms of gastroparesis." *Am Surg*, vol. 79, no. 5, pp. 457–464, may 2013. [Online]. Available: https://www.ncbi.nlm.nih.gov/pubmed/23635579

[35] S. Hackl, C. Lanschutzer, P. Raggam, and W. Randeu, "A novel method for determining the mutual inductance for 13.56mhz rfid systems," in *2008 6th International Symposium on Communication Systems, Networks and Digital Signal Processing*. IEEE, jul 2008, pp. 297–300. [Online]. Available: http://ieeexplore.ieee.org/lpdocs/epic03/wrapper.htm?arnumber=4610726

[36] H. Hwang, B. Jo, S.-W. Kim, J. Moon, and C. Kwon, "6.78 mhz resonance coupling for implantable medical devices," in *2015 8th Biomedical Engineering International Conference (BMEiCON)*. IEEE, nov 2015, pp. 1–3. [Online]. Available: http://ieeexplore.ieee.org/lpdocs/epic03/wrapper.htm?arnumber=7399554

[37] Y. Zhao, M. Nandra, C.-C. Yu, and Y.-c. Tai, "High performance 3-coil wireless power transfer system for the 512-electrode epiretinal prosthesis." *Conf Proc IEEE Eng Med Biol Soc*, vol. 2012, pp. 6583–6586, 2012. [Online]. Available: http://dx.doi.org/10.1109/EMBC.2012.6347503

[38] U.-M. Jow and M. Ghovanloo, "Modeling and optimization of printed spiral coils in air, saline, and muscle tissue environments." *IEEE Trans Biomed Circuits Syst*, vol. 3, no. 5, pp. 339–347, oct 2009. [Online]. Available: http://dx.doi.org/10.1109/TBCAS.2009.2025366

[39] M. J. Ferrua and R. P. Singh, "Modeling the fluid dynamics in a human stomach to gain insight of food digestion." *J Food Sci*, vol. 75, no. 7, pp. R151–62, sep 2010. [Online]. Available: http://dx.doi.org/10.1111/j.1750-3841.2010.01748.x

[40] P. Du, G. O'Grady, J. U. Egbuji, W. J. Lammers, D. Budgett, P. Nielsen, J. A. Windsor, A. J. Pullan, and L. K. Cheng, "High-resolution mapping of in vivo gastrointestinal slow wave activity using flexible printed circuit board electrodes: methodology and validation." *Ann Biomed Eng*, vol. 37, no. 4, pp. 839–846, apr 2009. [Online]. Available: http://dx.doi.org/10.1007/s10439-009-9654-9

APPENDICES

A. STIMULATOR PROGRAM

```
Gastrostimulator Program

#include <xc.h>
#include <string.h>
#include <stdlib.h>
#include <stdio.h>
#include "config.h"
#include <stdint.h>

#define _XTAL_FREQ 1000000

void frequency(void);
uint8_t changeMode(void);
volatile int count=0;
long int freq = 0;
int flag=0;
int value_low=0, value_high=0;

void init(void)
{
    TRISA   = 0b00100000;       // Pin 5 is the output pin for stimulation pulses
    LATA    = 0b00000000;
// Input output configuration
    ANSELA = 0x00;
    TXCKSEL = 0b1;              // TX Function is on RA4
    CCP1SEL     = 0b0;          // CCP1 is on RA2 (Pin 5)
    CCP1CON     = 0b00011100;
    CCPR1L      = 0b00000001;
    T2CON       = 0b00000011;
    OPTION_REG  = 0b00000000;
    TMR0        = 194;
    TMR0IE      = 1;
    PORTA =  0x00;
}

void main(void)
{
    init();
    OSCCON  = 0b11011011;
    __delay_ms(2000);

    // Timer1 configuration

    T1CONbits.TMR1CS = 0b10;   // clock timer with FOSC/4
    T1CONbits.T1CKPS = 0b00;//Pre scaler 1:1
    T1CONbits.nT1SYNC = 1; //Asynchronous mode selected
    uint8_t mode = 0b001;
    int modeset = 0;
    PR2 = 255;
    value_low = 50;
    value_high = 2500;
    PORTAbits.RA0 = 0;
    PORTAbits.RA1 = 0;
    PORTAbits.RA4 = 0;

    frequency();

    while(1){
                if(freq>=6775000 && freq <=6785000)
                {
                   mode = 0b010;
                   modeset = 1;
                }
                else if (freq>6700000 && freq <6775000)
                {
                   mode = 0b001;
                   modeset = 1;
                }
                else if (freq>6785000)//&& freq <6860000
                {
                   mode = 0b011;
```

```
                    modeset = 1;
                }
                else
                {
                    modeset = 0;
                    PORTAbits.RA4 = 1;
                }

                mode = changeMode();
                if(mode == 0b001)
                {
                    PR2 = 255;
                    value_low = 50;
                    value_high = 2500;
                }
                else if (mode == 0b010)
                {
                    PR2 = 140;
                    value_low = 500;
                    value_high = 2500;
                }
                else if ( mode == 0b011)
                {
                    PR2 = 72;
                    value_low = 2000;
                    value_high = 2500;
                }
                else
                {
                }

                if(TMR0IE == 1 && TMR0IF == 1 && modeset ==1 )
                {
                    count++;
                    if(count == value_low)
                    {
                        T2CON = 0b00000011;
                    }
                    else if(count == value_high)
                    {
                        T2CON = 0b00000111;
                        count = 0;
                    }
                    TMR0IF=0;
                }
            }
}
// This function counts the carrier frequency

void frequency(void){
    long int frequency[5], dummy=0;
    int i=0;
    char sStr[10];
    __delay_ms(100);
    for(i=0;i<5;i++)
       {
            T1CON = 0b10010101;   // Enable Timer 1
            __delay_ms(4);
            T1CON = 0b10010100;   // Disable Timer 1
            frequency[i] = TMR1;
            frequency[i] = frequency[i] *500;
            dummy=frequency[i];
            freq+=frequency[i];
            TMR1 = 0;
            __delay_ms(100);
       }

       freq=freq/5;         // Average the counted frequency
       __delay_ms(100);
}
```

```
143
// This function changes the modes of the stimulator

uint8_t changeMode(void){

        uint8_t bitPos = 0;
        uint8_t bitValTemp = 0b000;
150     long counter = 0;
        uint8_t flag=0;
        int bitSetFlag = 0; // false by default

        __delay_ms(2000);
        for(bitPos=0;bitPos<3;bitPos++)
        {
            bitSetFlag =0;
            do
            {
160             frequency();
                if(freq >1280 && freq < 1300 && bitSetFlag == 0 )
                {
                    counter++;
                    if(counter >= 30)
                    {
                        bitValTemp |= (1<<bitPos);
                        bitSetFlag =1;
                        flag = 1;
                    }
170             }
                else if (freq >1250 && freq < 1270 && bitSetFlag == 0 )
                {
                    counter++;
                    if(counter >= 30)
                    {
                        bitValTemp &= ~(1<<bitPos);
                        bitSetFlag =1;
                        flag = 2;
                    }
180
                }
            }while(!(freq >1310 && freq < 1330) || !(bitSetFlag == 1));

        counter = 0;
        bitSetFlag =0;
        flag =0;
    }
    return bitValTemp;
}
190
```

B. MAPPING ROBOT INTERFACE

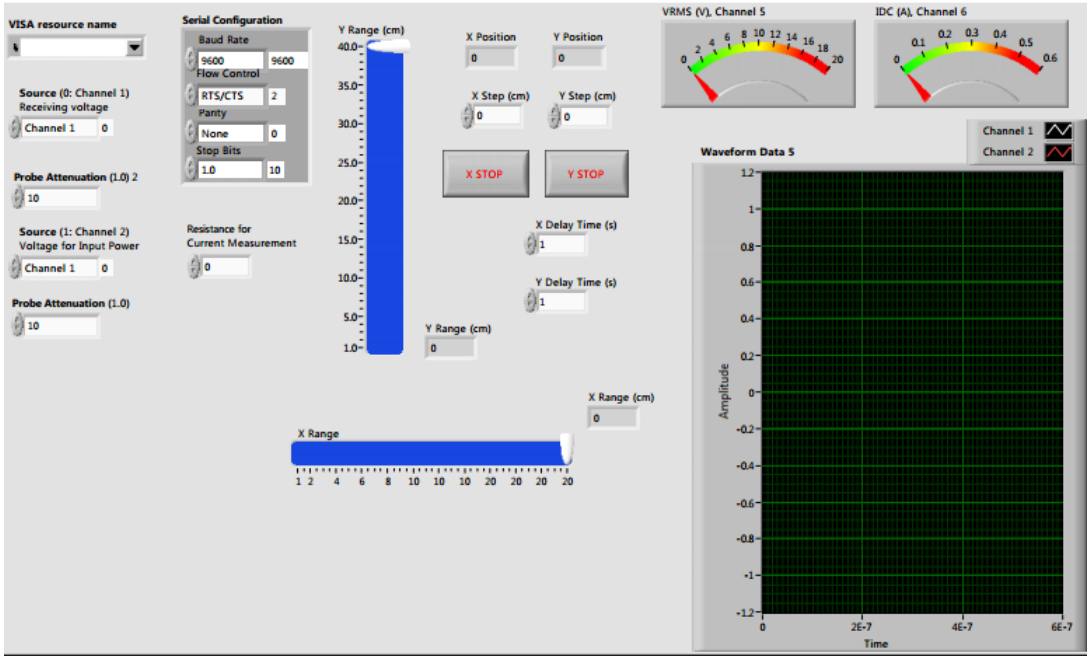

Fig. B.1. LabVIEW user interface for the field mapping robot.